Office of Naval Research
Department of the Navy
Contract N6onr-244
Task Order II

AN EXPERIMENTAL STUDY OF CENTRIFUGAL PUMP IMPELLERS

A. J. Acosta
R. D. Bowerman

Hydrodynamics Laboratory
California Institute of Technology
Pasadena, California

Report No. E-19.8
August 1955

Approved by:
A. Hollander

Office of Naval Research
Department of the Navy
Contract N6onr-244
Task Order II

AN EXPERIMENTAL STUDY OF CENTRIFUGAL PUMP IMPELLERS

A. J. Acosta
R. D. Bowerman

Hydrodynamics Laboratory
California Institute of Technology
Pasadena, California

Report No. E-19.8
August 1955

Approved by:
A. Hollander

CONTENTS

I. INTRODUCTION

This report summarizes about three years of experimental work on centrifugal pump impellers by the hydraulic machinery group of the Hydrodynamics Laboratory. Some of the work discussed herein has already been reported as individual investigations by this project.[1,2,3,4] This report embodies these earlier results together with more complete and recent investigations of centrifugal pump impellers.

In the past, industry has developed a line of highly efficient pumps by considering only gross effects by a one-dimensional theory and then resorting to empirical development based on many years of experience in order to obtain acceptable designs. This procedure is partly justified by the fact that there is little actually known about the internal flow in pump passages even though the body of fluid dynamic theory is available and applicable. The problem of turbomachine design (and in particular centrifugal pump design) is complicated by the fact that only a relatively few of the factors involved can be included in a practical mathematical or analytical solution. However, the basic difficulty facing any rational analysis has been the lack of knowledge of the important internal flow details. Thus in most instances the general applicability of analytical results must be left open until sufficient experimental evidence is available.

One of the objectives of an experimental program on pump impeller research must be, therefore, to obtain a sufficient amount of information on the internal and over-all flow characteristics so that their main features become clear and are understood. Although such knowledge may only substantiate design practices developed by experience, this result would in itself be of considerable interest. Moreover, this type of information, which is not generally available, makes possible, through the knowledge of the experimental coefficients found, extension of designs into new fields of application.

The preceding discussions outline the motivation for the work reported herein. A series of experiments was conducted on four "two-dimensional" impellers in which the inlet angle was the only variable. These data include head, torque and efficiency measurements in addition to internal loss, velocity profiles and pressure distributions. As an aid in the qualitative

description of the flow, photographic techniques were also used.

Meridian cross section profiles of impellers range from those of the very narrow width, radial flow, through the Francis or mixed-flow type of impeller sections built on cones, and ultimately to the straight axial profile. Attention in the present work has been confined to that of the "three-dimensional" or Francis impeller in which the meridian flow is generally curved but leaves radially. The flow pattern for such geometries is quite complex, so, in order to reduce the variables involved, "two-dimensional" impellers were made. These test impellers have plane, annular shroud shapes with a fairly quick transition from the axial to radial direction at the inlet. Such shapes are of limited practical application; however, they are of value in experimental work because of the relative ease of observation and measurement offered. Thus, in order to complete the investigation, additional work was carried out on a "three-dimensional", high efficiency, commercial impeller with similar operating characteristics, and the results compared with those of the two-dimensional experiments.

II. DESCRIPTION OF LABORATORY FACILITIES, INSTRUMENTATION AND IMPELLERS

Facilities

A detailed description of the Laboratory facilities may be found in Refs. 1 and 2, so that only the salient features will be mentioned here. The test facility consists of a closed hydraulic circuit using water as the fluid medium with a circulating pump, venturi flow meters and a system of piping to distribute the flow to any one of three test basins in which the experimental models can be installed. Although the flow may be made to circulate either direction through the test basin, for pump work the circuit is arranged so that flow approaches the impeller axially and leaves radially, discharging into the test basin at atmospheric pressure. The impellers are driven by a vertically mounted d.c. dynamometer which is equipped with an accurate speed control. Figure 1 shows the impeller and test basin arrangement and Fig. 2 is a view of the experimental setup.

Impellers

In this program two types of impellers were used: a two-dimensional design with parallel shrouds, and a well-designed commercial three-dimensional or Francis type runner. A series of four of the two-dimensional

impellers were used, each of which had the shroud inlet design shown in Fig. 3. The unconventional shape of the eye resulted from a desire to have a symmetric flow at the vane inlet edges. These impellers form a series of similar designs all with the same radius ratio, breadth and exit vane angle but with systematically varied inlet angles.

In order to obtain a smooth and systematic variation of blade angle from inlet to exit, it was first assumed that the relative flow followed the blade shape exactly (i.e., an infinite number of vanes) and then the growth of the whirl or tangential component in the absolute flow was specified. In this particular case a linear variation was chosen. Even though it was realized that the above assumption is incorrect, at least the resulting vane shapes are not completely arbitrary, and furthermore this procedure obviates shapes with excessive curvature. The details of the calculations are given in Appendix I and a summary of the various impeller geometrical constants are tabulated in Table I below. Inasmuch as only the impeller inlet angles are different for the four runners, they will be designated by these values throughout the test.

TABLE I - Impeller Geometrical and Design Constants

	Two-Dimensional				Three-Dimensional
Inlet Angle β_1 (impeller designation)	20°	17°	14.5°	12.5°	23° *
Outlet Angle β_2	23.5	23.5	23.5	23.5	17°
Radius Ratio (r_1/r_2)	0.583	0.583	0.583	0.583	0.525*
Outlet breadth/outside diameter (b_2/D_2)	0.086	0.086	0.086	0.086	0.116
Design Flow Rate ϕ (shockless inlet)	0.117	0.100	0.083	0.067	
Number of vanes	6	6	6	6	5
Outside diameter	10.30"	10.30"	10.30"	10.30"	12.875
K_1 (Appendix I)	1.660	1.868	2.134	2.490	

*Suction shroud values.

Impeller Manufacture

The shape of the two-dimensional impeller series made fabrication particularly simple. The top shrouds were turned from lucite to permit photographic and visual observations to be made, and the bottom shroud was black anodized aluminum. The vanes were rolled to shape from 3/32-in. 2-S aluminum sheet, or from brass sheet in some cases, and were recessed in slots milled in the shrouds, six equally spaced vanes being employed in each case. The resulting impeller assembly was held together with 3/32-in. through bolts at the exit edge of the individual blades. For reasons of economy, two sets of slots were installed in each of two sets of shrouds, the unused slots being waxed-in during operation. An assembled impeller is shown in Fig. 4.

Test Setup

The impeller was installed in the basin as shown in Fig. 2. Since only low rotative speeds were used, sealing was not a problem and in all cases running clearances of about 0.010 in. were found to be satisfactory. The flow from the impeller discharges into a set of parallel diffusor shrouds which serve to guide the flow and eliminate exterior disturbances.

In operation, the water surface was maintained slightly above the level of the impeller. The impeller was operated at a constant speed of 225 rpm. The flow rate was regulated by a manual throttle valve in the suction line and the speed-controlled circulating pump.

Instrumentation

Two types of information were sought in this work: first, the overall operating characteristics, i.e., head, torque, and flow rate; second, internal flow data, viz., pressure distributions, velocity and total head loss profiles.

a. Flow Rate. The volume flow rate was established and measured by any one of the three venturi meters available and a differential mercury manometer.

b. Torque. The reaction torque of the motor case was balanced by graduated weights connected to the dynamometer torque arm by means of a wire and pulley system. A Statham electric strain

gage attached to the arm was used as an indicator for the null position. Mechanical stops limit the motion to a few thousandths of an inch and protect the gage. The strain gage output was read by an optical galvanometer. Thus the procedure consisted of balancing the torque with small weights until the null position was achieved. This arrangement allows torque to be measured with zero displacement, thus minimizing bearing friction. The resultant sensitivity of the system was about 1/500 of the full scale reading. With the relatively small torques measured in these tests (1.5 ft. lb. max.), vibration was found to be a problem so that in order to improve accuracy several readings at each operation point were taken and averaged.

With the setup employed, the tare reading was fairly large. In particular, the bearing friction and water drag on the shroud surfaces were large and as they took no part in the pumping operation their corresponding torques were treated as a tare.

c. Head. The head developed by the impeller was measured with a water-air manometer and total head probes, one being installed in the impeller inlet, or eye, and the other mounted at the impeller discharge. Both simple impact probes and Kiel venturi-type total head probes were used at the impeller exit and were usually installed only 1/16 in. away from the vane tips.

d. Internal Flow Measurements. All of the internal flow measurements consist of pressures (except the photographic observations[1]) and hence a device to measure these pressures quickly and easily is necessary. For the work in this Laboratory it was found to be expedient to use a manometer attached to and rotating concentric with the impeller.[3,4] The manometer employed consisted of thirty 6 mm tubes about 18 in. long with a common manifold to all tubes. One tube was reserved for a reference pressure (which was taken to be the inlet total head) and others were connected to various static or total head piezometer connections. Thus, with a maximum economy of effort, static pressure distributions, relative velocities and relative "energy losses" could be found.

Static piezometer taps in the vane surfaces were installed by drilling down the breadth of the vane to an 0.030-in. perpendicular hole, and by soldering 1/16-in. brass tubing into vertically milled slots on the vane surface before it was bent to the proper contour. Both methods were found to be practicable.

Relative velocity heads were obtained with 1/16-in. simple impact probes mounted in the impeller passages and directed into the relative flow. In order to prevent flow asymmetry, such tubes were usually distributed throughout all of the passages.

It should be noted that the rotating manometer does not give the static pressure distribution directly and that in order to obtain it the centrifugal effects in the connecting tubing must be accounted for (Appendix II).

e. Flow Visualization. The lucite shrouds of the test impellers permit both visual and photographic observation, as described in Ref. 1. Briefly, these techniques consist of injecting immiscible liquid globules into the flow and observing their subsequent history either in the relative or absolute reference frames. Both motion pictures and multiple flash exposures on a single plate were taken. There was also some use made of stereographic photography.

Flow visualization by these methods has been found extremely valuable for qualitative exploratory investigations and provides a necessary complement to the internal flow measurements.

f. Accuracy. Both the flow rate and speed were capable of being measured with an error of less than 1/2 percent. However, due to the large tare, torque values were only known to within 1.5 percent or so. The greatest difficulty was experienced in the determination of the pump head. Since the head reading varied somewhat over the passage height and depended also on the distance away from the impeller exit, there is some question as to what value of "head" should be used. The over-all accuracy of the performance measurements is thus about three to four percent, depending somewhat on the value of the head.

Most of the relative measurements cannot be accurately

determined. Instrumentation errors, manometer errors, etc., probably are within two percent for the most part and such variation would be typical of the pressure distribution results also. Flow asymmetries, incorrect angles on the relative total head tubes, etc., could cause additional errors that are quite difficult to detect.

III. EXPERIMENTAL WORK

A. Description of Tests and Results

Complete characteristic diagrams for the four two-dimensional impellers are presented in Fig. 5 in terms of the dimensionless developed head coefficient ψ_d, torque coefficient τ, flow-rate coefficient ϕ and efficiency η. As mentioned in the preceding paragraphs, there is some arbitrariness in the definition of the impeller head. In particular, it was found that the distance between the discharge total head probe and the impeller periphery was important. Figure 6 shows this variation with the probe 1/6 and 3/8 in. from the impeller exit. The major difference is seen to occur at flow rates less than the design point. At such low flow rates, considerable mixing and other real fluid effects can come into play since the path lines between the impeller and probe are long, flat spirals. Thus, in the rest of this work the 1/16-in. position was used as a standard. Any additional losses due to equalization and mixing of the flow are therefore not counted in the determination of head or efficiency.

For purposes of comparison, the developed head is plotted vs. flow rate for all four impellers (Fig. 7) and efficiency vs. flow rate in Fig. 8. Figure 9 shows the "input" head or work coefficient $\psi' \left(= \psi_d/\eta \right)$ vs. ϕ for the four impellers together with a theoretical estimate.[6] Similar data were also taken on the three-dimensional impeller studied, and are shown in Fig. 10. Performance data for other similar three-dimensional impellers may be found in Ref. 2.

The design flow rate for the two-dimensional impellers is designated by ϕ_e on Figs. 7 - 9 and was obtained by making the inlet relative flow angle equal to the inlet vane angle with the assumption that there is no prewhirl. It is realized that this procedure is inaccurate for potential flow[5,6] but as the basis of a comparative study it should suffice. Typical inlet and outlet velocity triangles for a pump are shown in Fig. 11.

Pressure distribution data on the blade surfaces were obtained only for the 20° and 12.5° impellers. A typical piezometer tap drilling schedule for the 20° impeller is shown in Fig. 13 and the static pressure distributions are given in Figs. 14 and 15.

Viscous and real fluid effects are most readily shown by contour plots of energy loss or defect. It can be shown (Appendix II) that the head difference between any total head tube in the relative flow and the inlet total head as read on the rotating manometer represents a loss of energy in the flow due to friction. In the remainder of this report "loss" refers to loss of relative total head (i.e., $p/\rho g + \frac{1}{2g} W^2$). Energy loss contours are given in terms of the percent of input head or work coefficient for the 20° impeller for various flow rates at the exit section of the passage (Fig. 16), for the 15° impeller at the exit and mid-radius position (Fig. 17), and for the 12.5° impeller at three locations, i.e., exit (Fig. 18), mid-radius (Fig. 19), and inlet (Fig. 20). Static pressure distributions between the vanes along top and bottom shrouds were also taken for the 12.5° impeller, so that with the aid of the loss coefficients relative velocities in the passage section could be computed. Velocity profiles across the height of the passage and for several positions between the vanes are given for the 12.5° impeller at three radial stations in Fig. 21.

Similar data were also taken for the three-dimensional impeller. Loss contours at the exit are shown in Fig. 24 and at the inlet in Fig. 25. Relative velocity computations were also made at the exit section, but due to the high curvature of the meridian flow at the inlet, static pressures could not be measured there, hence velocities could not be determined. It should be mentioned that the three-dimensional impeller performance was obtained with a setup quite similar to that of the other impeller (Fig. 2), i.e., with plane annular diffuser shrouds. However, the exit loss measurements had to be made without the top shrouds. Additional work was also done on the effect of these shrouds by removing the bottom shroud as well.

The results of these tests and their interpretation will be discussed in the following section.

B. Discussion

1. Over-all Characteristics

It is immediately clear from the plots of head vs. flow rate for the four impellers in Figs. 7 and 9 that the inlet angle has a profound effect upon the entire characteristic. In general, the best efficiency point is

seen to move to the left (Fig. 8) for the reduced inlet angles, as would be expected. At relatively high rates of flow (ϕ = 0.1 - 0.12) larger heads are seen to be developed for the high inlet angles than for the smaller ones, and the slope of the H-Q curve progressively steepens as the inlet angle is reduced. The developed head for all impellers is seen to be more or less the the same at about ϕ = 0.06, indicating that in this region the flow does not depend much on the inlet angle.

It should not be assumed that the losses which occur away from the best efficiency point are solely responsible for the variations in performance even though this assumption is commonly found in pump literature.[7] An inspection of the brake horsepower or torque coefficient for the four impellers (Fig. 5) shows that the input work is different for each of them. The maximum peak value goes from about τ = 0.061 for the 20° impeller to about 0.051 for the 12-1/2° impeller, and the flow rate coefficient for the maximum decreases from 0.135 to 0.11. The difference between each of these quantities is thus on the order of twenty percent. It is clear then, from the torque characteristics, that attributing the variations in head performance to internal fluid losses cannot alone explain the discrepancies. It should be pointed out also that inlet blade angle variations of the magnitude in these tests can only account for about 1 or 2 percent change in the H-Q characteristic on the basis of potential flow calculations.[10] Also it is of interest to note that in each case the maximum efficiency is seen to fall to the left of the maximum torque.

The design points of these impellers were taken to be the flow rate for shockless entry as calculated by the elementary one-dimensional theory. Vector velocity triangles for the impeller inlet and outlet are shown in Fig. 11. In order to show the influence of local angle of attack or incidence angle to the blade inlet edges, the angle of attack for the 90 percent efficiency range vs. flow rate is plotted for each of the four impellers in Fig. 12. The angle of attack for the best efficiency point is seen to vary from - 2° for the 20° impeller to about 1-1/2° for the 12° impeller. From the slope of the 90 percent envelope it is doubtful whether an impeller with a 10° inlet angle would ever achieve this efficiency. Again, this observation is taken to be a result of operation at extremely low flow rate coefficients and not primarily a result of the inlet angle. This effect also shows up in the fact that the ratio of the high efficiency operating range to the design flow rate is smaller

for the low angles than the larger ones. If the inlet angle of attack were the sole criterion, it can be easily shown that this ratio should increase as the inlet angle is reduced.

Correlation with Potential Flow Theory. In Figs. 7 and 9 are shown theoretical $\psi - \phi$ curves computed on the basis of potential flow theory.[6] Although these ideal characteristics were determined for logarithmic spiral vane shapes, it can be shown[10] that small perturbations in inlet angle will not materially affect the $\psi - \phi$ characteristic. The outstanding feature on both of these figures is the rather large discrepancy in slope between the ideal performance and both developed and input heads. The same phenomenon was also noticed in Ref. 5 in which a series of experiments was conducted on 30° log-spiral, two-dimensional impellers. In this work the discrepancy was attributed to the influence of the inlet boundary layer arising from the sharp turn.

In Fig. 9 it is seen that the design points of the four impellers all fall nearly on the computed characteristic. It is clear that the experimental $\psi' - \phi$ curves must intersect the ideal $\psi - \phi$ characteristic at some flow rate. However, the coincidence of the design ψ' values with the computed characteristic must be regarded as fortuitous, at least for the present. This question will be considered again when the three-dimensional impeller results are discussed.

2. Pressure Distribution Measurements

Knowledge of the static pressure distributions on the vanes gives a direct measurement of the vane loading, and hence evaluation of the design of the blade shape. Pressure distribution measurements on the 20° impeller were first reported in Ref. 4, and additional measurements on the 12.5° impeller are reported herein.

In both Figs. 14 and 15 it is seen that the pressure distributions or loading curves near the design point are relatively smooth and show no unusual reversals. This fact is, no doubt, a consequence of the smooth curvature of the vanes, and supports the contention that for radial flow machinery, the exact blade design is not of paramount importance provided abrupt changes in curvature are avoided, and that the blade angle smoothly increases or decreases.

"Shockless" Flow Rate. As mentioned before, the design points of these impellers were chosen so that the relative flow would stream smoothly onto the leading edge with no velocity discontinuities. The flow rate for this operating condition is termed "shockless entry" in the pump literature. For the 20° impeller the nearest approach to shockless entry occurs about $\phi = 0.140$, whereas according to the simple theory, shockless entry should occur at $\phi = 0.117$. Thus, shockless entry occurs at a flow rate greater by 20 percent than that computed on thebasis of the infinite vane theory. According to potential flow calculations[6, 10] the shockless flow rate for this impeller geometry should be 32 percent greater than that based on the infinite vane theory. It seems reasonable that boundary layer blockage and other real fluid effects could account for the relatively small discrepancy between this and the observed value. Similar results were also observed in Ref. 5 in experiments conducted on impellers with 30° log-spiral vanes.

The pressure distribution measurements of Fig. 15 on the $12\text{-}1/2^{\circ}$ impeller show that shockless entry is about at $\phi = 0.06$, whereas the design calculations were for $\phi = 0.067$. This result does not fall on the trend established by the 20° impeller[5] or the theoretical predictions. It has already been observed that at such low flow rates, real fluid effects become of increasing importance. It should not be surprising, therefore, that such a different behavior could occur under these circumstances.

Loading Distribution. At or near the shockless entry operating point it is clear from the head-flow rate characteristic that the vanes of the 12.5° impeller are considerably less loaded than those of the 20° impeller. The fact is reflected in the pressure distribution diagrams which are slimmer and more elongated for the smaller angle. As previously noted, the load distributions for both of these impellers is "reasonable" near shockless, indicating that as long as the change in angle from inlet to outlet is not rapid and continuously increases (or decreases), any blade design should be satisfactory. This observation is mainly qualitative and is principally intended to point out the difference in importance that the vane shape has for axial and radial pumps. It will be shown later that the 12.5° impeller, although having a smooth increase in vane angle, does have certain undesirable internal flow features as compared with the 20° impeller.

At flow rates less than shockless entry, large velocity discontinuities

are seen to appear at the inlet on both impellers. In a similar fashion at high flow rates, the distributions on the two faces intersect and cross over.

Operation at Low Flow Rates. It is clear that at shockless entry there is a stagnation point at the leading or inlet edge of the blade. As the flow rate is reduced, it is evident from the pressure distributions and also from physical considerations that the stagnation point moves onto the leading or pressure face of the blade. This point continues to move away from the inlet edge toward the outlet as the flow rate is reduced until shut-off has been reached. The final position of the stagnation point depends upon the blade angle, radius ratio, etc. Thus, whatever the particular design, back flow can occur over a considerable extent of the pressure side of the blade at low flow rates. Such back flows are not conducive to high efficiency or stable operation. The excessive path length and highly unfavorable pressure gradient that must exist may cause large scale separation and other real fluid effects. At shut-off these effects become even more predominant. Motion pictures show that, in general, the fluid in the inner portions of the impeller rotates like a solid body and that an irregular pulsating rotation opposite to the direction of impeller rotation occurs at the exit. This sequence of events which occurs as the flow rate is lowered, as determined by motion pictures, is that a separation zone appears first on the suction side of the blade. With a further decrease in flow rate, alternate passages are seen to "stall out" completely, the flow then being much like a solid body rotation. The stalled pattern seems to be stable with respect to the impeller and does not propagate around the periphery as is observed in axial flow compressors.[11] This situation occurs at about a flow rate of $\phi = 0.05$ or so and can be verified by the pressure distributions taken in alternate passages on the 20° impeller shown in Fig. 14. This configuration remains until the flow rate becomes very low, and finally near shut-off all the passages stall out with the inner portions rotating like a solid body. Near the exit there is a large-scale irregular eddy rotating in the opposite sense to the impeller direction. The pressure distributions for $\phi = 0$ are shown in Figs. 14 and 15. It can be seen that at the inlet the static pressure is near zero and is considerably below the forced vortex line, indicating that there is little or no rotation of the fluid in the impeller eye. From the inlet edge to about $r/r_2 = 0.8$ the pressure is distributed like that of rigid body rotation and the small loop in the discharge portions represents the work going into the eddy maintained at the exit.

Cavitation Susceptibility. The knowledge of the pressure distributions permits one to make some estimation of the cavitation susceptibility of an impeller. In terms of the pressure coefficient C_p it can be shown that the value of Thoma's σ for the inception of cavitation is

$$\sigma_{inception} = \left| \frac{C_{p(min)}}{2\psi} \right|$$

where ψ is the head coefficient. For the 20° impeller near the design flow rate ($\phi = 0.117$) this becomes

$$\sigma_{incpt.} = \frac{0.3}{(2)(0.5)} = 0.3$$

and at shockless entry

$$\sigma_{incpt.} = 0.10.$$

It is interesting to note that as the flow rate is reduced from shockless, the absolute value of the minimum pressure continues to increase and the values of $\sigma_{incpt.}$ increase. However, when stall is encountered, $|C_{p\ min}|$ decreases, and near shut-off even becomes slightly positive. This means that lower absolute pressures are required for cavitation inception at very low flow rates than at the design points. This situation is in contrast to that of the axial flow pump which requires increasing suction pressure to prevent cavitation as the flow is reduced.[7]

Unfortunately, this knowledge of the noncavitating pressure distribution tells nothing of the performance during cavitating conditions or of cavitation "breakdown" or choking. However, from the shape of the pressure curves one can make some rough deductions: At or near shockless entry the pressure distributions are smooth and the pressure is nearly constant on the suction side. If this pressure is below the known vapor pressure of the liquid, the fluid must boil or cavitate. For a first approximation, the work represented by the area between the vapor pressure line and the pressure loop is not put into the flow as head. An inspection of these distributions at low flow rates shows that there are quite sharp pressure peaks of small area. Hence, one would infer that less head may be lost when cavitating under such circumstances than at shockless, although

cavitation inception occurs sooner. According to these ideas, serious cavitation from the standpoint of head loss would not occur before $\sigma = 0.08$ or so at a flow rate coefficient of $\phi = 0.117$ for the 20° impeller. For the given characteristics of this impeller, this value agrees with the expected cavitation performance as given in Ref. 7, page 267.

3. Internal Flow Measurements

Loss Contours. The internal velocity and relative total head profiles probably give the best indication of the location and magnitude of real fluid effects possible with the experimental setup. The energy loss contours at the exit section for the 20° impeller (Fig. 16) give a qualitative idea of the distribution of these effects for various flow rates. In these and the following contour plots, the loss in relative head is expressed as a fraction of the total developed head. It can be seen that up to and somewhat beyond the design point the regions of high loss are concentrated on the trailing (suction) side of the vane. At higher flow rates, the low loss fluid moves over to the leading (pressure) side of the passage in accordance with the adverse negative angle of attack existing then at the vane inlet edge.

Loss contours are also shown for the 15° impeller at a high flow rate (about 70 percent greater than design) midway through the passage ($r/r_2 = 0.75$) and at the exit (Fig. 17). The high rate of flow is responsible for gross separation and flow detachment seen in the loss contours at mid-radius.

It is well known that such nonuniformities in relative total head give rise to circulating or secondary flows perpendicular to the main stream direction. Such evidence is offered by the outlet survey of Fig. 17 which shows how the areas of high loss fluids have been distorted and displaced towards the trailing or suction side of the passage.

More extensive loss data are shown in Figs. 18-20 for the 12.5° impeller. Figure 18 shows loss contours at the exit ($r/r_2 = 1.00$) at various flow rates. A difference between these distributions and those of the 20° impeller is immediately clear, namely, that a zone of large energy loss is always located next to the trailing side of the vane, even for flow rates about 60 percent greater than the design. In fact, the percentage loss continuously increases with flow rate starting at the lowest value of $\phi = 0.048$.

The inner survey ($r/r_2 = 0.73$) of Fig. 20 shows, in general, a thick region of relative energy defect on the trailing side of the passage and on the bottom shroud. These loss distributions remain more or less unchanged until the flow rate exceeds about $\phi = 0.072$. At flow rate coefficients greater than this value, high loss areas are seen to occur on the pressure face of the vane. The pressure distribution data, (Fig. 15) for these flow rates show the static pressure curves on leading and trailing blade surfaces of the inlet crossing over at about this flow rate, so that unfavorable incidence angles occur at the inlet. Any further increase in flow rates results in regions of extreme loss probably associated with local flow detachment.

This sequence of events is roughly followed by the internal surveys at $r/r_2 = 0.89$ (Fig. 19) except that, in general, the profiles indicate greater losses near the trailing surfaces and less near the pressure (leading) surface. This behavior may be expected to follow from the general shape of the leading pressure distribution curves.

Thus, it can be seen that the exit surveys on the 12.5° impeller do not follow the trend established by the inner surveys or the 20° impeller. The possibility that the flow separates along the trailing side of the vane near the exit immediately suggests itself. The velocity surveys discussed in the next paragraph further support this idea.

To a certain extent the use of "percentage loss" is illusory in this connection. To get an idea of the absolute magnitude of the loss the change in total head must be accounted for.

Velocity Profiles. From the loss measurements and static pressure determinations on the impeller top shroud it is possible to calculate the relative velocity in the passage. Figure 21 presents this information as relative velocity plotted against the channel height for several stations across the passage. An outstanding feature of each of these diagrams is that the velocity profile near the suction side of the vane progressively deteriorates from the inner to the outer radial stations. In fact, for all flow rates except the very highest the velocity distributions near the exit strongly suggest that flow separation occurs near there. The other salient feature of Fig. 21 is the pronounced boundary layer that appears on the lower shroud at the inner radius at a flow rate coefficient of about $\phi = 0.06$. Also interesting is the "inverted" shape of the exit velocity profiles some-

what above the design point. It would appear that the low energy regions are being centrifuged out of the impeller. This behavior has been noted before on rotating shrouds with no blades.[12] wherein it was observed that a substantially separated main stream could be stabilized and re-attached by sufficient shroud rotation.

Loss Coefficients. With the velocity profiles having been determined, it became possible to calculate weighted loss coefficients through the impeller. A true loss coefficient would be weighted with the radial velocity to account for variations in work of each fluid stream. Because flow angle was difficult to measure, the loss coefficients were computed with relative velocity. Consequently, for flow rates much different from the design condition, errors must occur and the resulting value must be too low. Figure 22 shows this coefficient for the inlet and exit stations as a function of flow rate. At the design point it is seen that about sixty percent of the total loss through the impeller has occurred at the inlet station $r/r_2 = 0.73$. It is interesting to note that the inlet loss rises sharply either side of the design point. The exit loss coefficient fails to show a rise for flow rates less than ϕ_e probably because of the aforementioned errors incurred in the weighting procedure. At the design point, however, computation of efficiency by means of the weighted loss coefficients agrees to within a percent or so with the measured value.

Comparison of Two-Dimensional Impellers. The over-all characteristics of the four two-dimensional impellers are similar and show the trends to be expected from the progressive decrease in inlet vane angle. The internal flow patterns are unquestionably different, however, because of their different torque or brake horsepower curves (Fig. 5). Qualitative information to this effect is offered by the loss contour plots of the 20° and 12.5° impellers. It is seen that, in general, fluid of low energy tends to be concentrated more behind the trailing side of the vane for the 12.5° impeller than the 20° one for all flow rates. Because of this fact the 12.5° impeller actually shows separated profiles near the exit at the design point, whereas the 20° impeller showed a much more uniform profile there. The difference is probably due to the excessive vane length of the 12.5° runner coupled with a continuous adverse pressure gradient.

It should be noted that separated flow in a pump will have a forced

vortex pressure rise through it rather than constant pressure as would be found on a stationary airfoil or blade of a cascade. The result is to centrifuge the separated region radially outwards. Thus, separation in radial flow machinery will not in general have as deleterious effects as it does in axial flow machinery.

4. Three-Dimensional Impeller Results

Overall Characteristics. In Ref. 2 Osborne and Morelli present complete characteristic data on several "three-dimensional" impellers, and the data on a 17° exit angle impeller is reproduced in Fig. 10. Figure 23 shows a profile sketch of the impeller. It is clear from Fig. 10 and those of Ref. 2 that the three-dimensional characteristics agree much better with the theoretical calculations than do the two-dimensional ones. The fact that the measured head on the 17° impeller is slightly higher than the theoretical prediction is not understood at the present time, and in Ref. 2 this difference is attributed to real fluid effects.

A surprising fact is that the head curves of the 17° three-dimensional impeller do not fall off with increasing flow rate as repidly as do the 23.5° two-dimensional impellers. This result appears (as is discussed below) to be due to the differences in inlet loss and velocity distribution of the two impeller types.

Internal Loss Distributions. Loss contours for different flow rates are shown in Fig. 24 at the exit and in Fig. 25 at the inlet. Near and above best efficiency conditions the exit contours indicate a moderate boundary layer on the bottom shroud and some concentration of loss near the trailing side. The inlet contours are instructive in that they show only moderate areas of loss at higher flow rates, confined for the most part to the bottom shroud and trailing side of the vane. From Figs. 25b, c, it is seen that the inlet edge of the vane behaves somewhat differently from top to bottom. Less loss is seen near the bottom shroud than near the top at $\phi = 0.12$ and vice versa for $\phi = 0.16$, indicating that not all sections of the inlet vane are designed to operate with the same inlet attack angle at a given flow rate. The discrepancy is not severe, however.

As mentioned in a foregoing section, the exit measurements were made with the top collecting plate removed as indicated in Fig. 23. This was

necessitated by the fact that the impact tubes were attached to the impeller exit by means of small brass blocks that protruded beyond the impeller. The water level in the test basin was normally such that the impeller was submerged with no possibility of air entering the passages. To investigate the influence of the bottom collecting ring, it was removed and the loss data were retaken. Surprisingly enough it was found that "negative" losses occurred over about 1/3 of the passage next to the pressure face of the vane and lower half of the passage for flow rates less than about $\phi = 0.10$. These values were far in excess of what could be accounted for by experimental error and based on $U_2^2/2g$ have maximum values of about $|\zeta| = 0.075$

It is known that if the flow proceeds from the impeller inlet to the exit, the loss must be greater than, or equal to, zero. Hence it is concluded the negative losses arise from an external recirculating flow of higher relative energy. This situation could occur if fluid of small absolute velocity (and thus higher relative total head) would circulate from the region exterior to the impeller discharge along the shrouds to the outer portions of the pressure side of the impeller blade. The flow picture would consist of loose spirals, part exterior and part interior to the impeller. The addition of a lower collecting ring substantially reduces the magnitude and extent of the negative losses. (This relatively small region occurs only for $\phi \leq 0.065$ is not shown in Figs 24). Presumably, it would be completely eliminated by the addition of a top plate as well.

This matter is of some importance since impellers frequently run in volutes with considerable side clearance. According to these observations the velocity distributions and presumably also the head would be slightly different for such operation.

Velocity Profiles. Static pressure measurements on the top shroud at the exit of the impeller were made and from these and the loss determinations, relative velocities were computed and are shown in Fig. 26. It was necessary to assume that the pressure was constant across the breadth of the impeller, but this should not introduce serious error into the results.

It can be seen from these figures that for $\phi \geq 0.10$ the velocity distributions are fairly flat between the blades except for a boundary layer region on the bottom shroud.

Due to the fact that the inlet portions of the impeller were strongly curved, the static pressure throughout the flow could not be measured. Thus it was not possible to present inlet relative velocity plots.

Discussion and Comparison of Two-and Three-Dimensional Impellers. Several of the salient differences between the two- and three-dimensional impellers have been mentioned already. Among the most important of these is the difference in the head and flow-rate characteristics. In fact, the flow rate for zero head of the 17° three-dimensional impeller is higher than any of the 23.5° two-dimensional impellers. Furthermore, the slope of the $\psi - \phi$ curve agrees much better with potential theory (as mentioned before) and also is less steep than the two-dimensional results.

The reasons for this behavior may be found in the inlet surveys for the two cases (Fig. 20 and Fig. 25). The abrupt turn of the two-dimensional impeller gives rise to the large inlet loss previously mentioned and a large boundary layer on the bottom shroud. This behavior occurs more or less throughout the entire region of good efficiency in the two-dimensional impellers, but for the three-dimensional impeller the inlet performance is seen to be good until the highest flow rate observed. A comparison of the two- and three-dimensional exit velocity profiles is shown in Figs. 26 and 27. It is seen that the two-dimensional runners do not have exit profiles as flat as the three-dimensional one. In view of these facts, the simplest over-all explanation would be that the influence of the boundary layer at the inlet and subsequent formation of a thick retarded zone on the low-pressure side of the vane lower the effective blade angle of the two-dimensional impellers and increase the radial velocity by the blockage of the passage. The direction of both of these effects is the same, i.e., to decrease the head at a given flow rate and to steepen the $\psi - \phi$ curve. These effects are larger for the 12° impeller than for the 20° impeller.

Thus, it is not surprising that steeper head flow rate curves can be exhibited by the two-dimensional impellers. In fact, the influence of inlet angle on the torque characteristics of the two-dimensional impellers has already shown that their effects on internal flow patterns are large. If, in addition, the head losses encountered at the inlet are considered, it is easy to see why the efficiency of the two-dimensional runners is not only lower but has a sharper peak as well.

In Ref. 2 experiments were done on two three-dimensional impellers that differed only slightly in the details of inlet construction, and it was found that there were significant differences in performance of the two runners. It was suggested there that large inlet losses were incurred as a result of the relatively minor inlet changes. That such a possibility can occur is borne out in the present report. Not only can losses occur, but the resulting change in flow pattern alters the basic performance of the machine.

Effect of Volute. It should be remembered that the present results are applicable only to impellers and not to a complete pump. Due to the effect of the case or volute, there are a number of operational features that are decidedly different between the free impeller and complete pump. However, at the design point and somewhat on either side the influence of the case is not marked[13] and the results of free impeller tests may be applied there. At flow rates much lower, and particularly much higher than the volute design point, significant deviations from the free impeller performance are found.

This discussion will be closed with a brief comment on operation at low flow rate coefficients, e.g., $\phi \leq 0.05$. As a general remark, the two-dimensional impellers showed less variation in head, velocity, etc., across the breadth of the impeller at the exit than did the three-dimensional impellers. Motion pictures of the flow[1, 2] also show substantial secondary flows in the three-dimensional impellers. A significant feature of the three-dimensional impellers at these flow rates is the sudden jump or discontinuity in the head produced and torque required.

This behavior may be attributed to three-dimensional flow effects arising from stalling or separation in the inlet portions of the blade. The exact sequence of events that follow from separation are poorly known apart from the fact that strong radial flows can take place. Probably the influence of the shroud shape, as such, is not crucial since mixed and axial flow pumps exhibit similar low flow rate characteristics. This problem is an important one since discontinuities in head and torque fix the limits of stable operation in pumping circuits.

5. Summary and Conclusions

From the experimental results reported herein it is seen that there are important differences between the three-dimensional (Francis type) and two-dimensional (cylindrical vane) impeller designs. These differences are characterized by:

1. A higher and broader range of efficiency is found for the three-dimensional impellers.

2. The head flow-rate characteristic of the two-dimensional impellers is steeper than that for the three-dimensional impellers (even for vane angles exceeding the three-dimensional values).

3. The performance of the three-dimensional impellers can be closely predicted by potential theory, whereas this cannot be done for the two-dimensional impellers.

Internal flow data show that energy loss at the impeller inlet is chiefly responsible for the differences in the two types of design. Characteristically, about one-half of the loss of the two-dimensional impellers occurs at the inlet. For the two-dimensional impellers it is found that as the inlet blade angle is reduced, the flow rate for maximum efficiency decreases the efficiency remaining about the same, but the range of flow rates (in percentage) for high efficiency is reduced.

APPENDIX I

Blade Design

It is assumed that the fluid is perfectly guided by the blades. The blade shape is then chosen to make the tangential or circumferential component of the absolute velocity increase linearly with radius. Thus, from the velocity triangle (Fig. 11) it can be seen that the equation of the streamlines or blade surface is

$$\tan \beta = \frac{dr}{r\, d\theta} = \frac{C_m}{U - C_u} \quad . \qquad \text{I - (1)}$$

For constant impeller breadth $C_m = C_{m2}\, r_2/r$. The growth of C_u is now specified as

$$C_u = K_1 (r - r_o)\omega$$

where K_1 and r_o are constants. Equation (1) can be integrated to obtain

$$\theta = \frac{U_2}{C_{m2}} \left[\frac{1 - K_1}{2} \left(\frac{r}{r_2} \right)^2 + K_1 \frac{r_o r}{r_2^2} \right] . \qquad \text{I - (2)}$$

The constant K_1 is evaluated at the impeller exit by stipulating the blade angle β_2 there, i.e.,

$$C_{u2} = U_2 - \cot \beta_2\, C_{m2} = K_1\, \omega (r_2 - r_o) \ ,$$

or,

$$K_1 = \frac{1 - \left(C_{m2}/U_2 \right) \cot \beta_2}{1 - r_o/r_2} \qquad \text{I - (3)}$$

The blade exit angle β_2 of all impellers was arbitrarily chosen as $\beta_2 = 23.5^\circ$. The four impeller designs were then obtained by selecting $C_{m2}/U_2 = 0.110$ with r_o/r_2 taking the values 0.55, 0.60, 0.65, 0.70, respectively. The inlet blade angle β_1 is given by

$$\beta_1 = \cot^{-1} \left[\frac{1}{0.110} \left(\frac{r_1}{r_2} \right)^2 \left[1 - K_1 \left(1 - \frac{r_o}{r_1} \right) \right] \right] \quad . \qquad \text{I - (4)}$$

The flow rate for "shockless" or smooth entry is designated as the design flow rate ϕ_e and is computed as that value for which the relative flow angle is equal to the blade angle (blade thickness is accounted for in this computation).

A summary of the design constants is given in Table I of the text.

APPENDIX II.

Measurement of Loss and Relative Velocity

The Bernoulli equation in rotating coordinates for a frictionless, incompressible flow is

$$p_s + \frac{\rho}{2}(W^2 - U^2) = \text{const.} = p_T \,. \qquad \text{II - (1)}$$

If the total pressure p_t and static pressure p_s are measured at the same point, then

$$W = \left(\frac{p_t - p_s}{\rho / 2} \right)^{1/2} \qquad \text{II - (2)}$$

The quantity $p_t - p_s$ can be read directly on the rotating manometer, or p_t and p_s may be read individually as was done in the present experiments.

If the flow is not frictionless, then Eq. (1) is modified by the loss in relative total head p_ℓ, i.e.,

$$p_t = p_T - p_\ell$$

where the subscripts are defined in notation, thus

$$p_s + \frac{\rho}{2}(W^2 - U^2) = p_T - p_\ell \,. \qquad \text{II - (3)}$$

The quantity p_ℓ is measured directly on the rotating manometer by comparing the total pressure p_t with the inlet total pressure p_T (both pressures being read at the same radius, i.e., the manometer radius).

The loss coefficient is defined as

$$\zeta_r = \frac{p_\ell}{\frac{1}{2}\rho U_2^2} \,,$$

and the static pressure coefficient is defined as

$$C_p = \frac{p_s - p_T}{\frac{1}{2}\rho U_2^2} .$$

Then the relative velocity, as a dimensionless quantity, can be calculated by solving Eq. II - 3 with the above substitution of dimensionless coefficients:

$$\left(\frac{W}{U_2}\right)^2 = \left(\frac{r}{r_2}\right)^2 - C_p - \zeta_r . \qquad \text{II - (4)}$$

Efficiency and Weighted Loss Coefficient

It can be shown that the impeller efficiency is

$$\eta = \frac{\psi_d}{\psi_d + \bar{\zeta}_{r/2}} = \frac{\psi_d}{\psi'}$$

where $\bar{\zeta}_r$ is a weighted loss coefficient defined as

$$\zeta_r = \frac{\int \zeta_r \, w \sin \beta \, d A}{\int w \sin \beta \, d A} \qquad \text{II - (5)}$$

both integrals being evaluated over the discharge area of the impeller. The angle β is the relative flow angle. Since this angle is difficult to measure, it is assumed constant over the passage cross section. This assumption can only be correct near the design or best efficiency point of the impeller. At other flow rates and in particular low flow rates, the result must be low. In the figures of the report, the loss coefficients are usually expressed as fractions of the head.

REFERENCES

1. Osborne, W. C. and Morelli, D. A., "Head and Flow Observations on a High-Efficiency Free Centrifugal-Pump Impeller," Trans. ASME, Oct. 1950.

2. Osborne, W. C. and Morelli, D. A., "Measured Performance of Pump Impellers," Paper No. 50-A-90 presented at Annual ASME Meeting Nov. 1950.

3. Beveridge, J. H. and Morelli, D. A., "Evaluation of a Two-Dimensional Centrifugal Pump Impeller," Calif. Inst. of Technology, Hydrodynamics Laboratory Report No. 90.

4. Morelli, D. A., "Pressure Distributions on the Vanes of a Radial Flow Impeller," Heat Transfer and Fluid Mechanics Institute, Stanford, Calif., 1951.

5. Acosta, A. J., "An Experimental and Theoretical Investigation of a Two-Dimensional Centrifugal Pump Impeller," Trans. ASME, July 1954.

6. Busemann, A., "Das Forderhohenverhaltnis Radialer Kreiselpumpen mit Logarithmisch-Spiraligen Schaufeln," ZAMM, Vol. vol. 8, p. 372, 1928.

7. Stepanoff, A. J., "Centrifugal and Axial Flow Pumps," Wiley, 1948.

8. Wislicenus, G. F., "Fluid Mechanics of Turbomachinery," McGraw-Hill, 1948.

9. Blom, C., "Development of the Hydraulic Design for the Grand Coulee Pumps," Trans. ASME, Jan. 1950.

10. Acosta, A. J., "Potential Flow Through Radial Flow Turbomachine Rotors," Calif. Inst. of Technology, Hydrodynamics Laboratory Report No. E-19.4, June 1954.

11. Iura, T. and Rannie, W. D., "Observations of Propagating Stall in Axial Flow Compressors," Calif. Inst. of Technology, Mechanical Engineering Laboratory Report No. 4, April 1953.

12. Tyson, H. N. Jr., "Experimental Study of Flow Between Centrifugal Pump Shrouds," Calif. Inst. of Technology, Hydrodynamics Laboratory Report No. E-19.6, July 1954.

13. Bowerman, R. D., "Effect of the Volute on Performance of a Centrifugal Pump Impeller," Calif. Inst. of Technology, Hydrodynamics Laboratory Report No. E-19.7.

NOTATION

A - area

C - absolute velocity

C_p - pressure coefficient = $p_s - p_t / \rho U_2^2/2$

H - head (ft)

H_d - head developed by impeller

Q - flow rate (ft^3/sec)

T - torque

U - tangential velocity of impeller ($r\omega$)

W - relative velocity

g - gravitational constant

p - pressure

r - radius

z - axial coordinate

α - angle of attack

β - vane angle

ζ - loss coefficient = $p_T - p_t / \rho U_2^2/2$ (measured in relative flow)

η - efficiency = $\phi\psi/\tau$

θ - angular coordinate

ρ - density

σ - Thoma cavitation parameter = $\dfrac{\text{inlet total head minus vapor pressure}}{\text{developed head}}$

ϕ - flow rate coefficient = $Q/A_2 U_2 = C_{m2}/U_2$

τ - torque coefficient = $T/\rho r_2 U_2^2 A_2$

ψ - head coefficient = $H/U_2^2/g$

ψ' - input head or work coefficient = τ/ϕ

ω - angular speed

Subscripts

d - denotes developed head

e - denotes design point for impeller

ℓ - denotes loss

m - denotes meridional (or radial) component

s - denotes static pressure

T - denotes total pressure (or head) in impeller inlet

t - denotes total pressure (or head) at any other location

u - denotes tangential component

1 - refers to impeller inlet

2 - refers to impeller exit

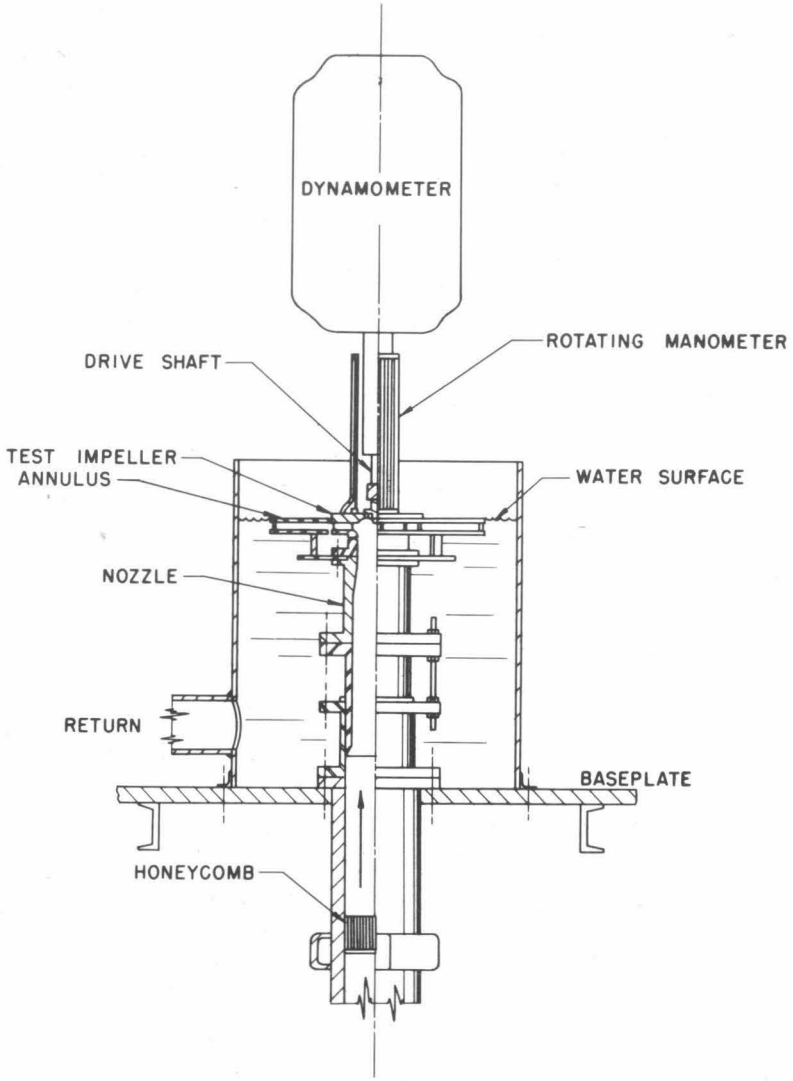

Fig. 1 - Cross section of impeller and test basin assembly.

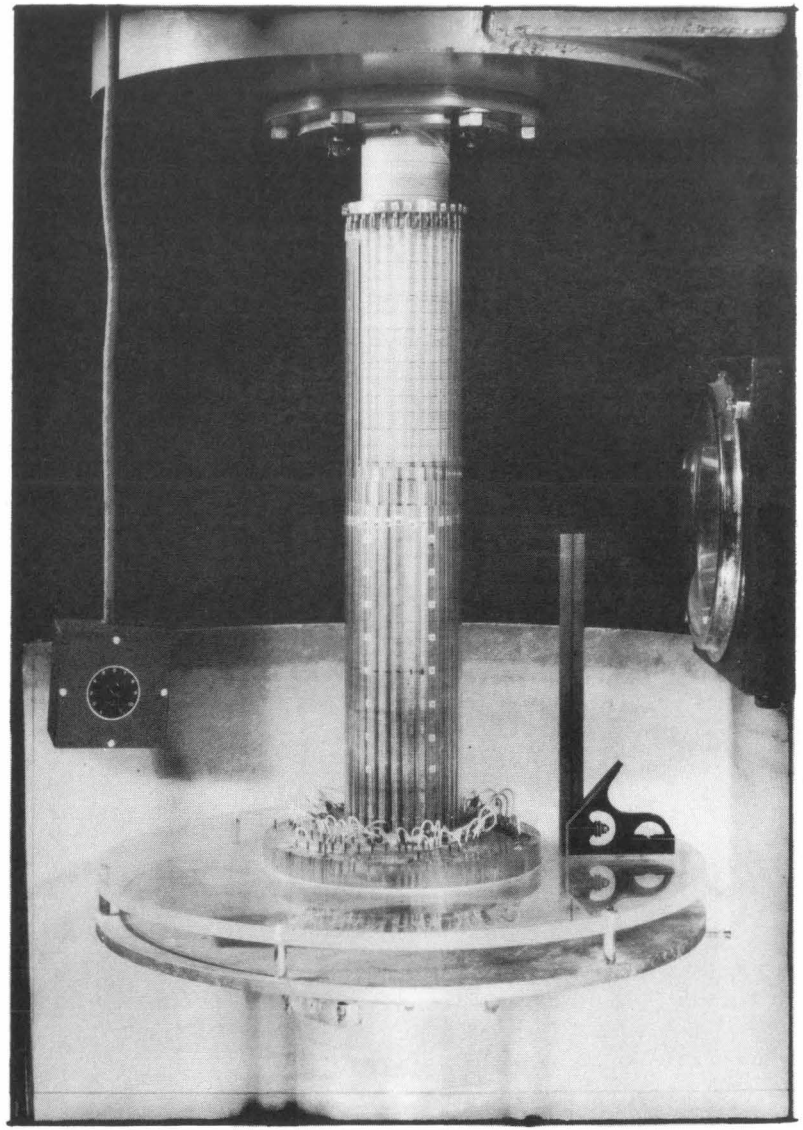

Fig. 2 - View of experimental setup.

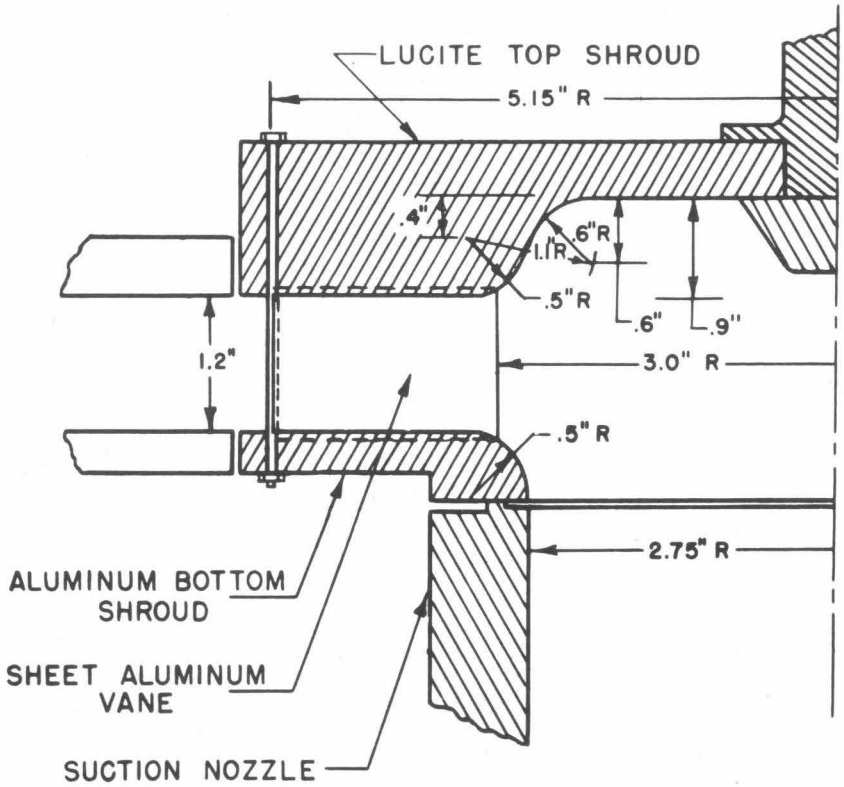

Fig. 3 - Cross section of two-dimensional impeller.

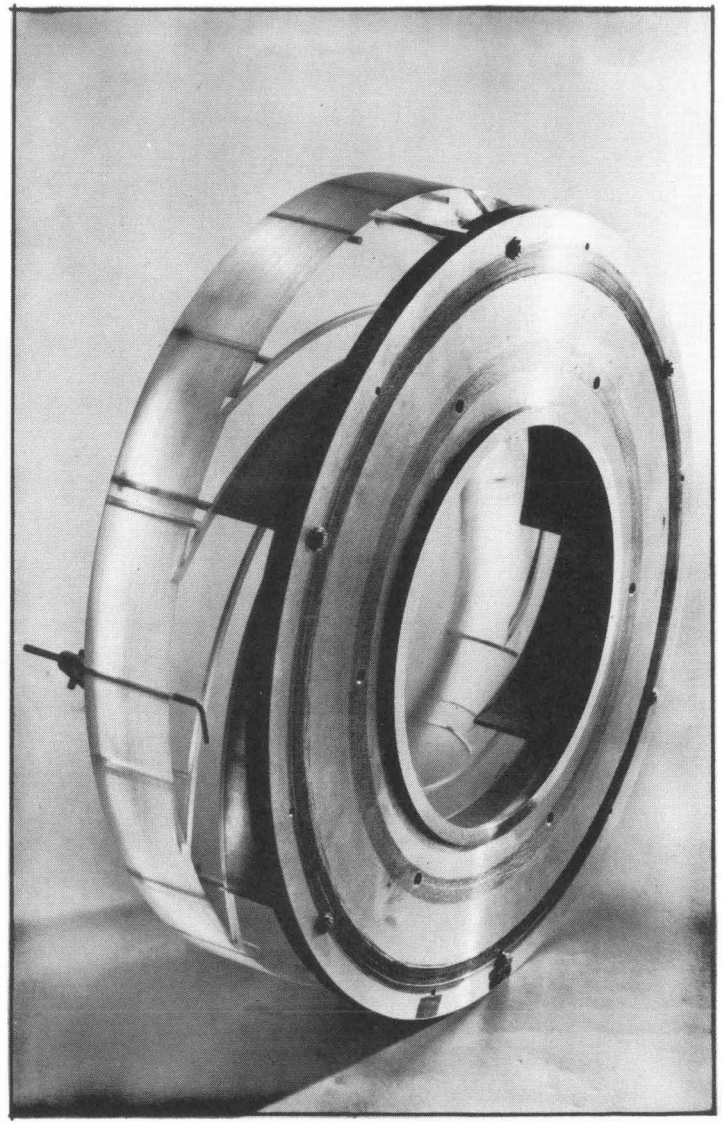

Fig. 4 - View of assembled two-dimensional impeller.

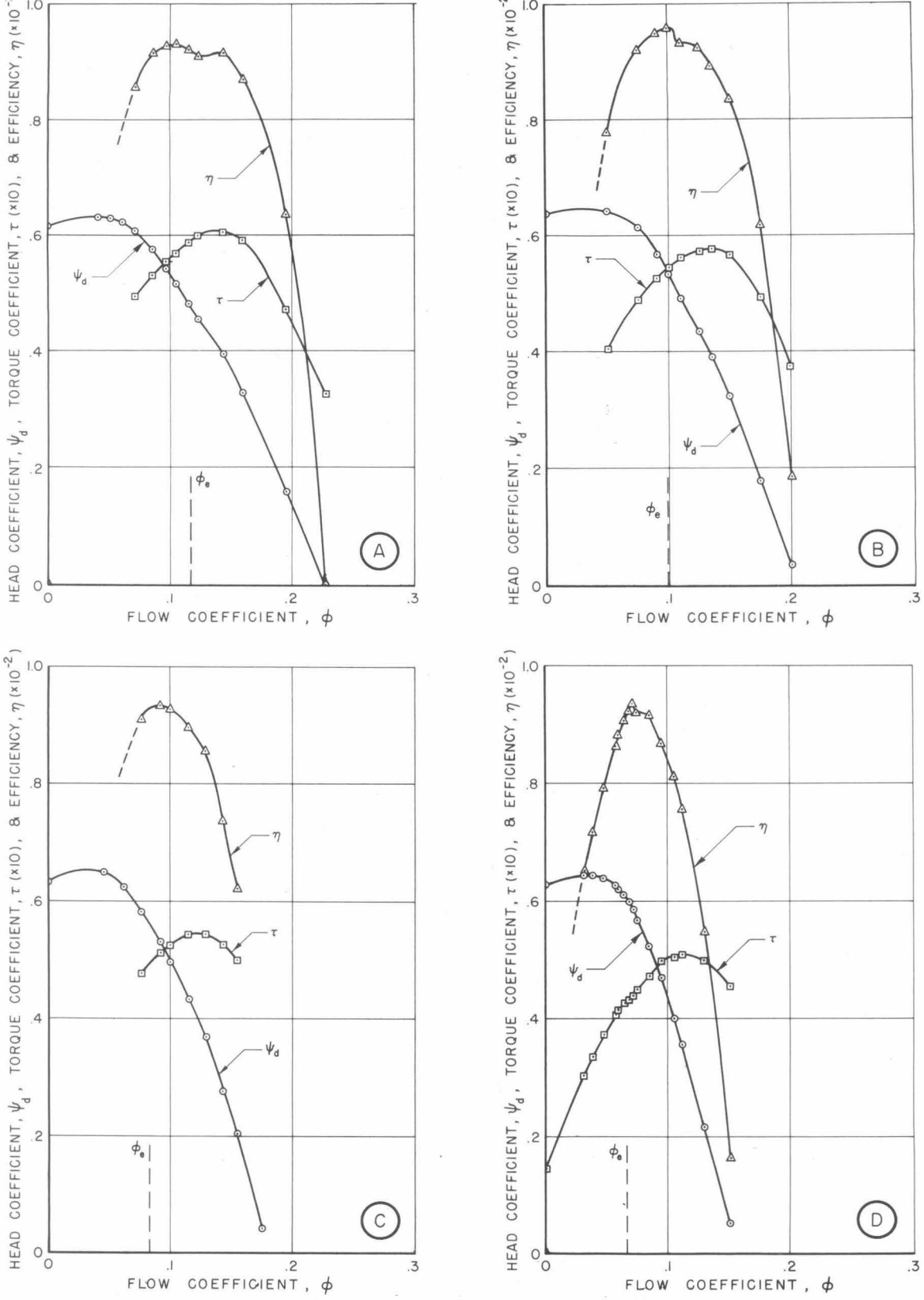

Fig. 5 - Head coefficient, torque coefficient, and efficiency vs. flow rate coefficient for the two-dimensional impellers.
Impellers, (A) 20°, (B) 17.5°, (C) 15°, (D) 12.5°

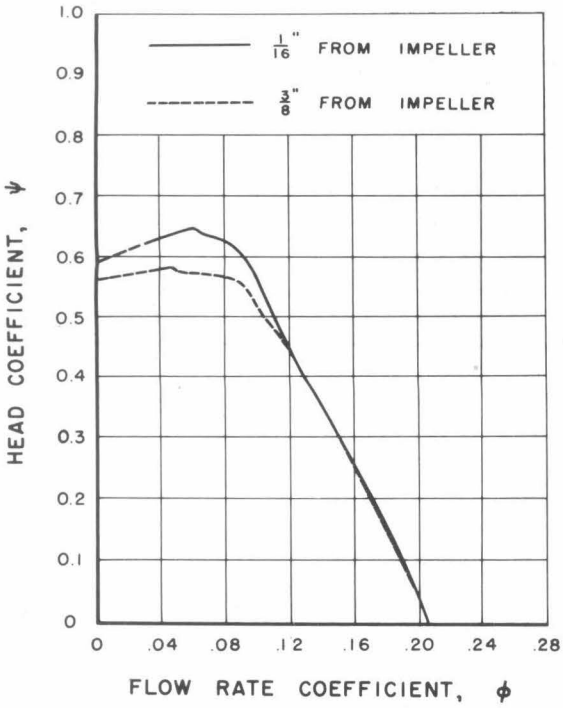

Fig. 6 - Developed head coefficient measured at 1/16 in. and at 3/8 in. radial distance from the impeller

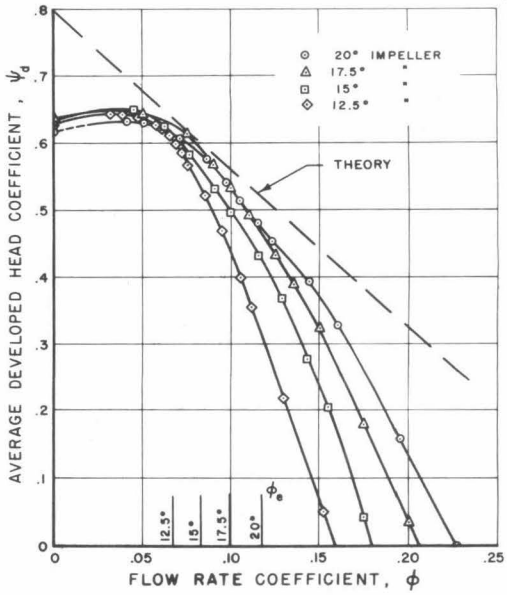

Fig. 7 - Developed head coefficient and theoretical head coefficient vs. flow rate coefficient for the two-dimensional impellers.

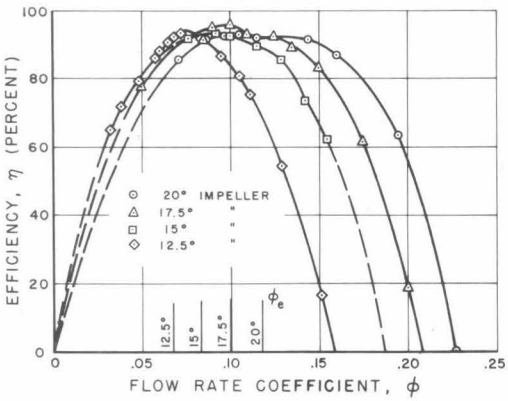

Fig. 8 - Efficiency vs. flow rate coefficient for the two-dimensional impellers.

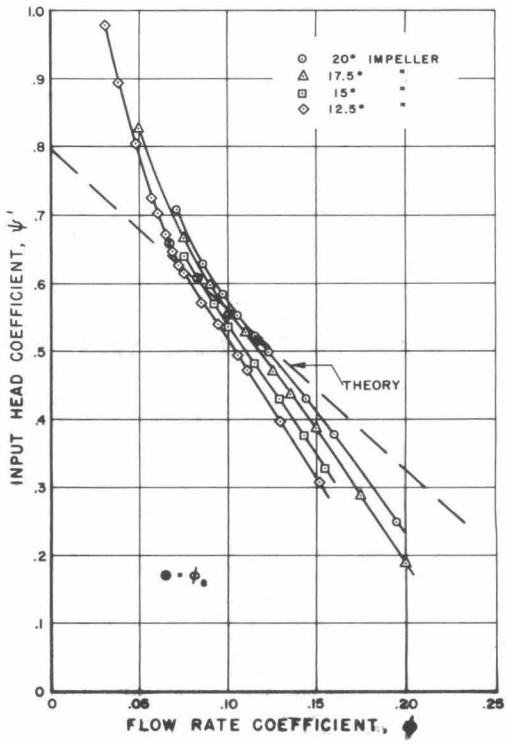

Fig. 9 - Input head or work coefficient vs. flow rate coefficient for the two-dimensional impellers.

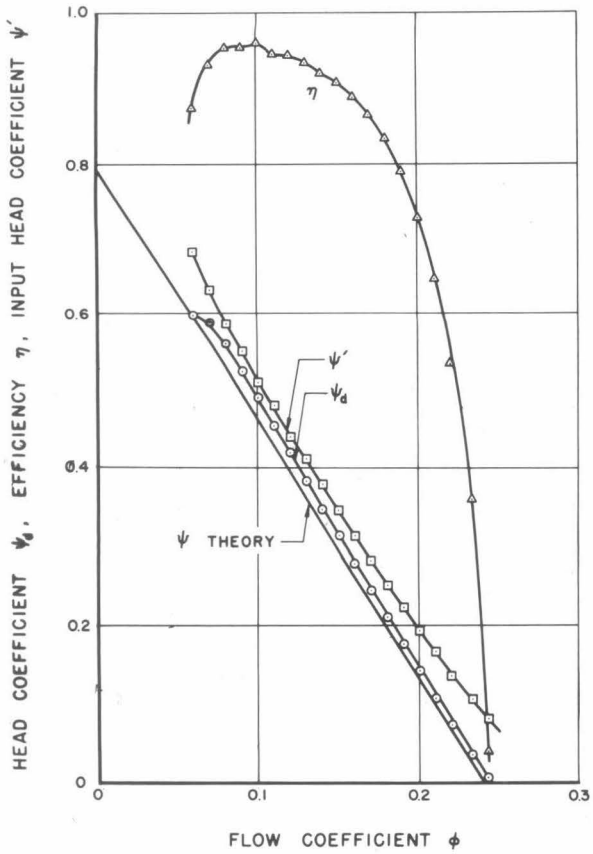

Fig. 10 - Head coefficient and efficiency vs. flow rate coefficient for the three-dimensional impeller.

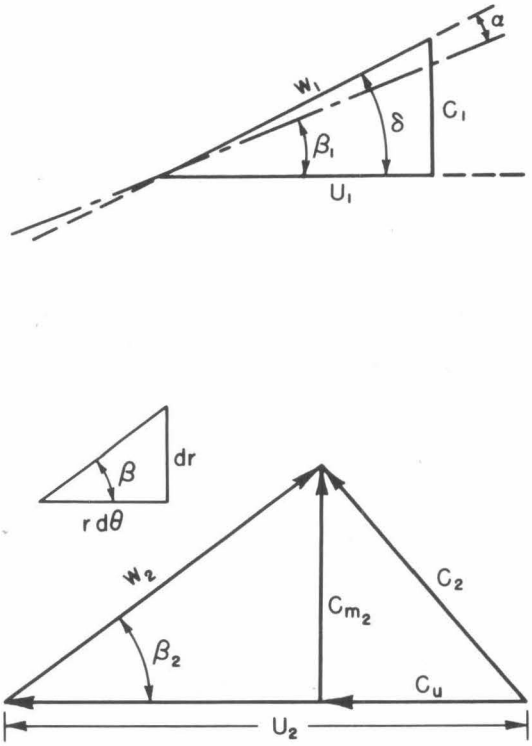

Fig. 11 - Inlet and exit velocity triangles.

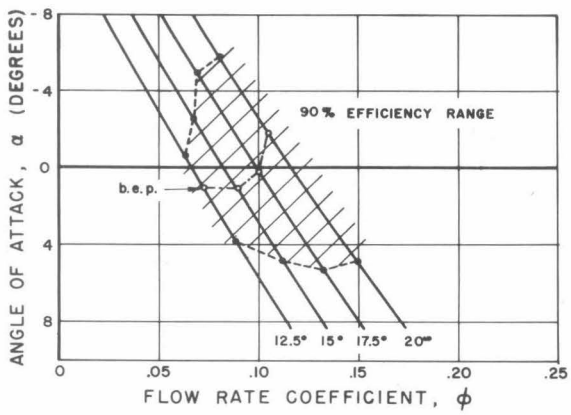

Fig. 12 - Inlet angle of attack vs. flow rate coefficient for the two-dimensional impellers.

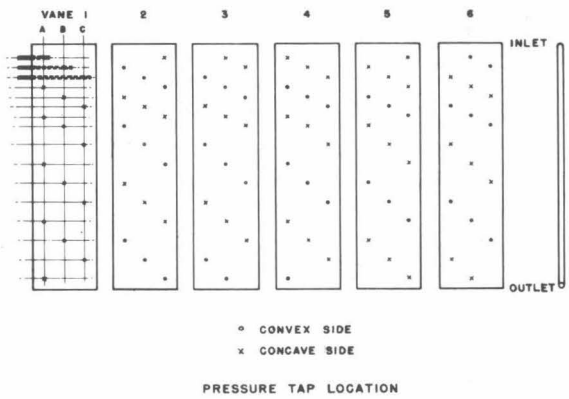

Fig. 13 - Piezometer tap drilling schedule for the 20° impeller vanes.

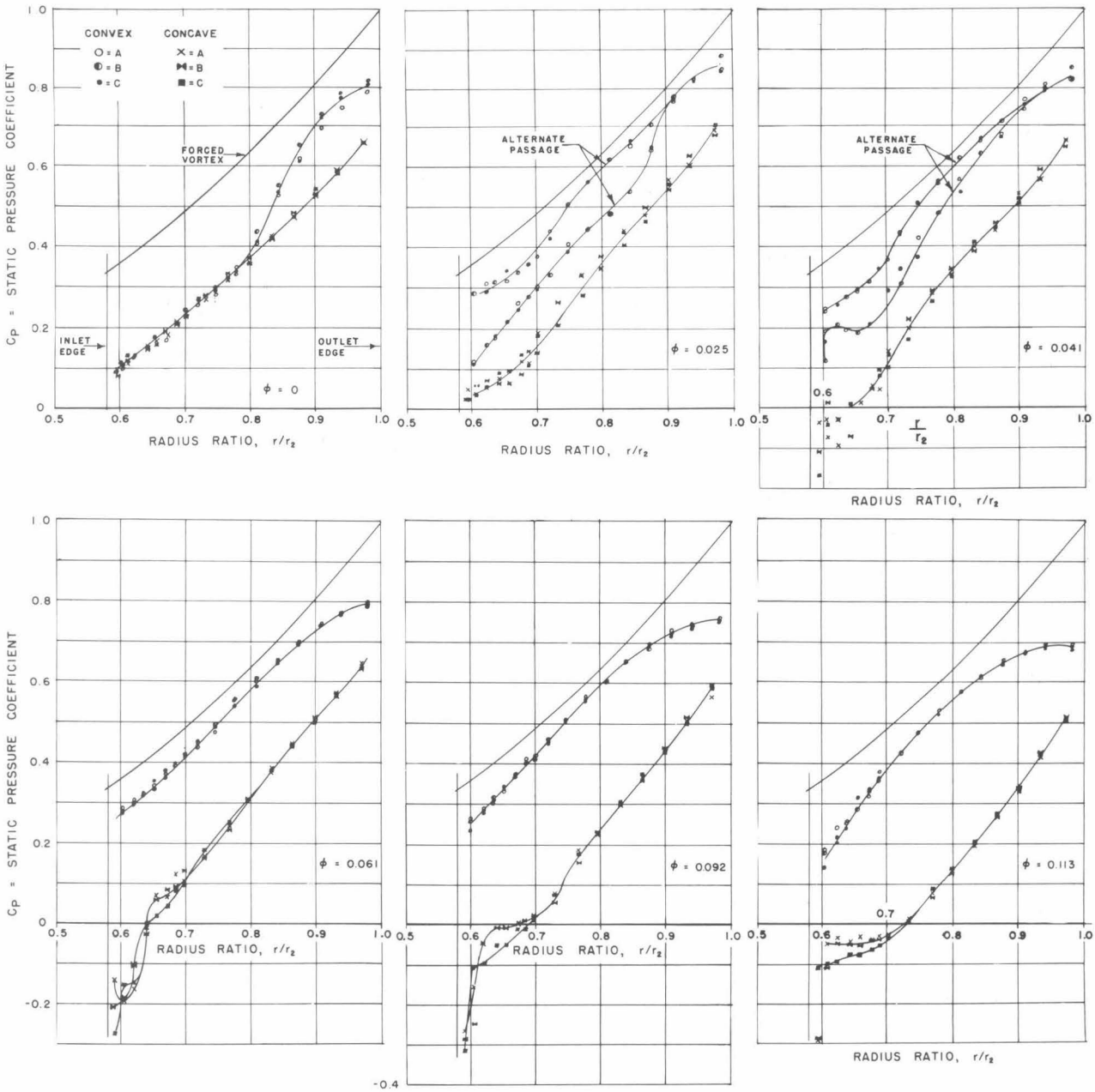

Fig. 14 - Static pressure distributions on the vanes of the 20° impeller for several flow rates.

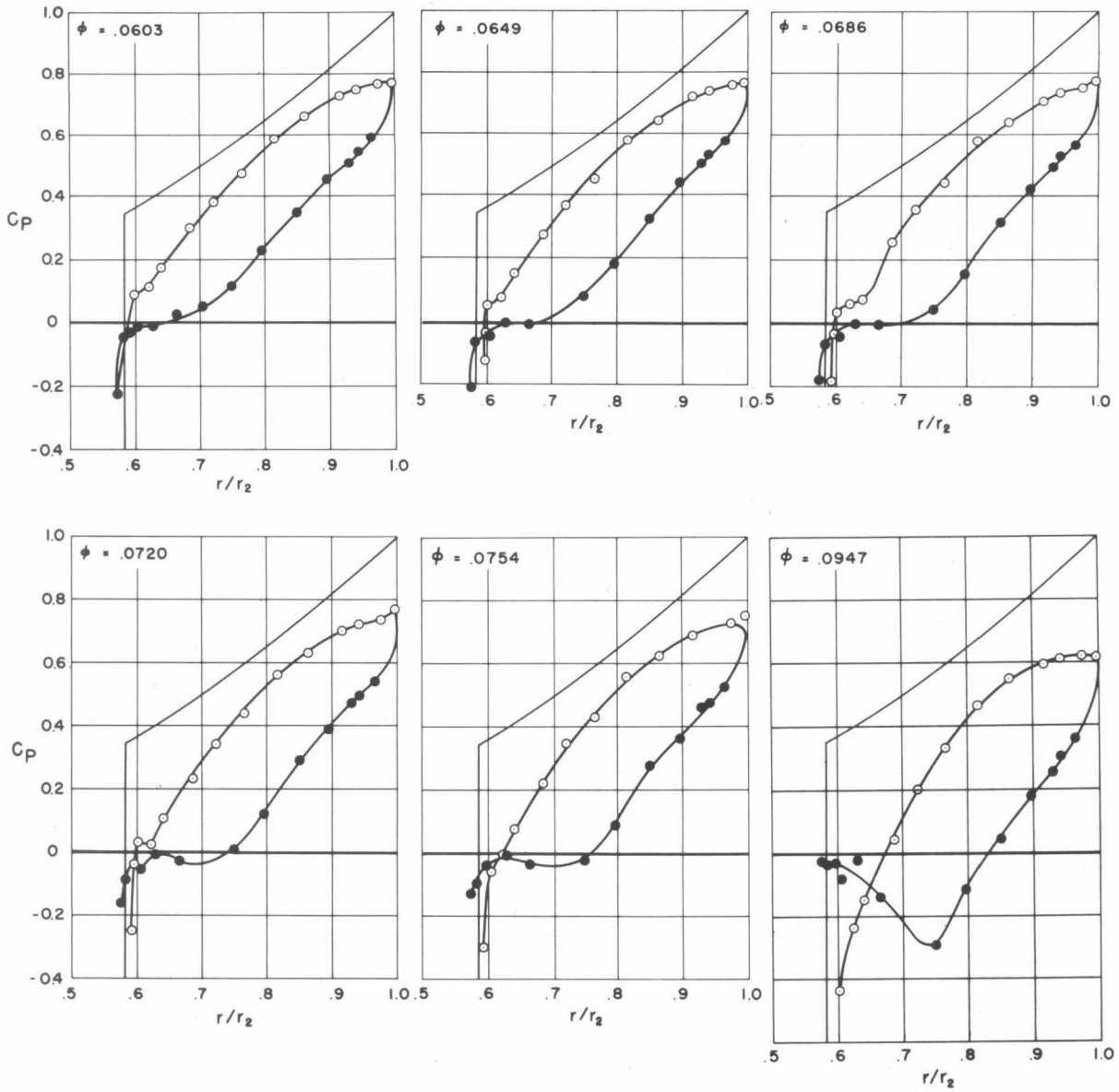

Fig. 15 (concluded) - Static pressure distributions on the vanes of the 12.5° impeller for several flow rates.

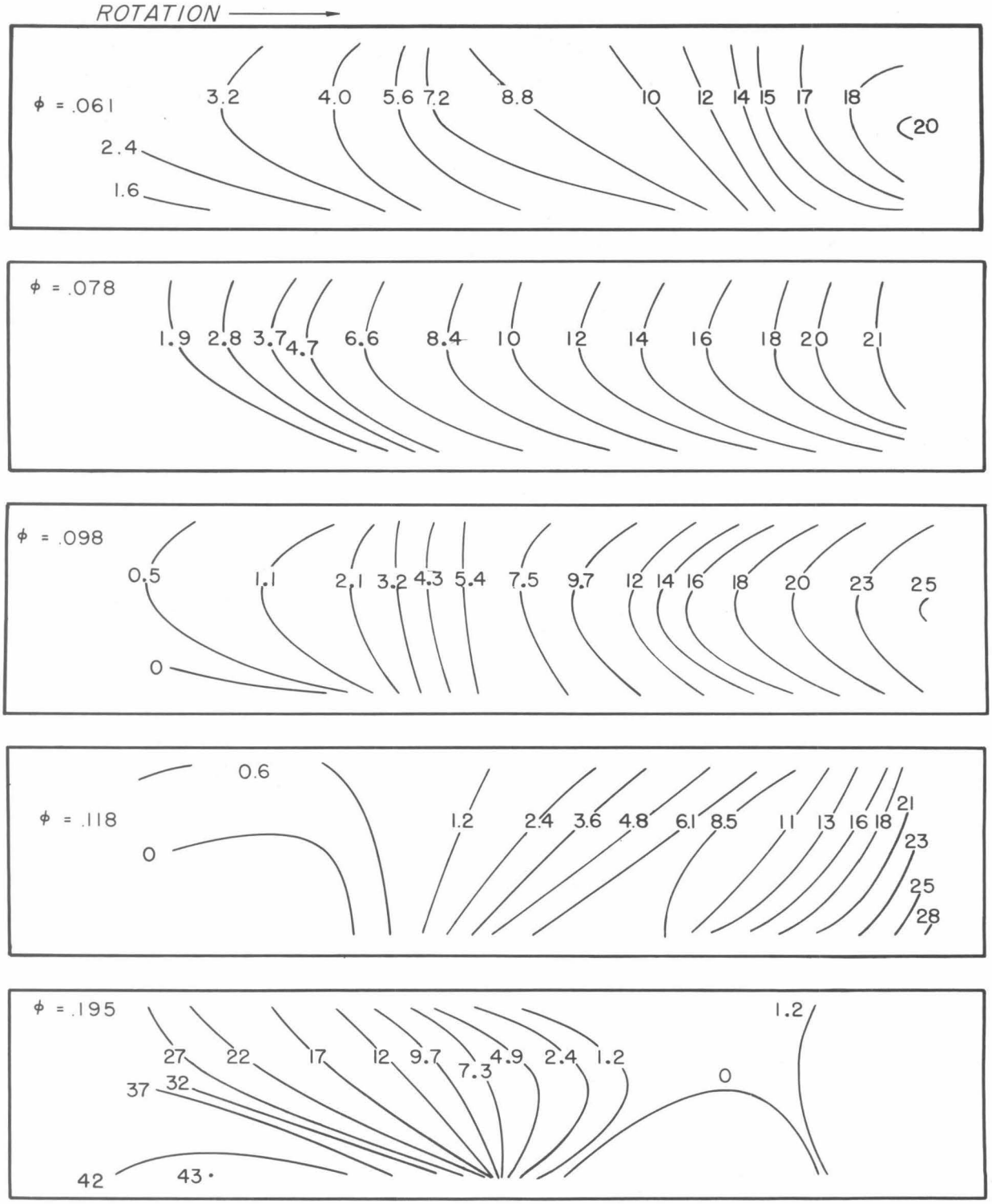

Fig. 16 - Relative total head loss contours for the 20° impeller at the impeller exit ($r/r_2 = 1.0$).

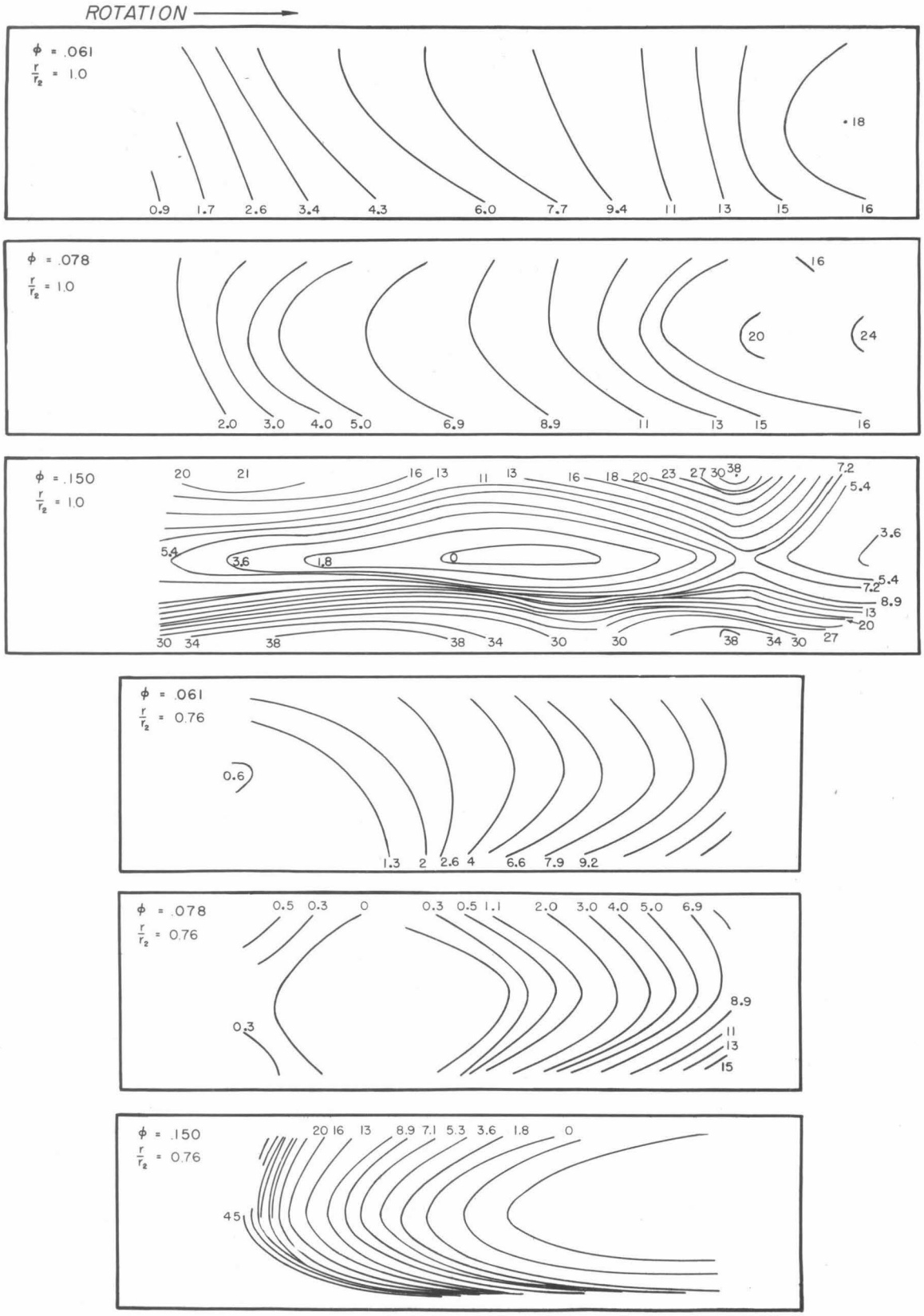

Fig. 17 - Relative total head loss contours at the exit ($r/r_2 = 1.0$) and mid-radius ($r/r_2 = 0.76$) for the 15° impeller.

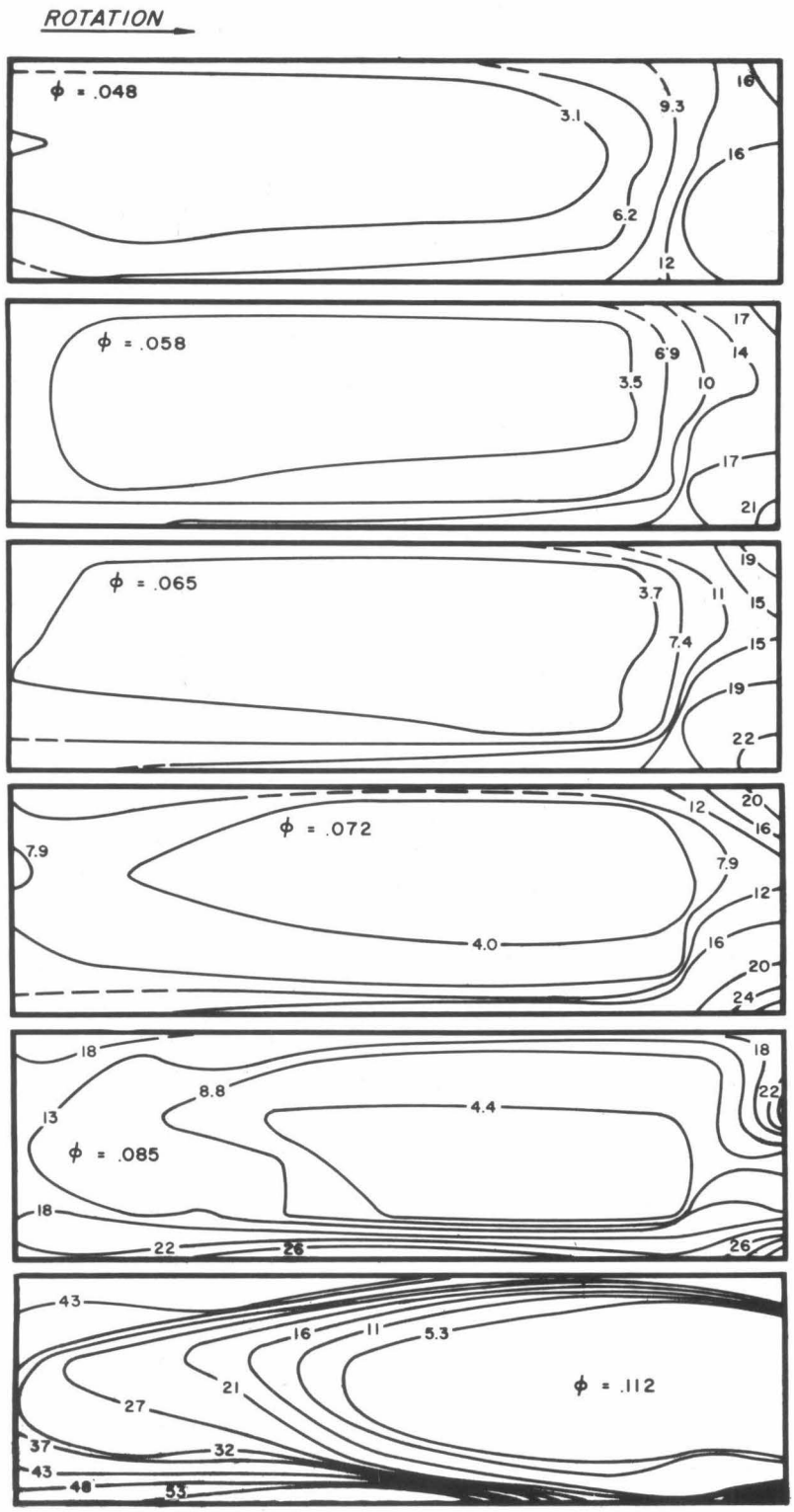

Fig. 18 - Relative total head loss contours for the 12.5° impeller at the impeller exit ($r/r_2 = 1.0$).

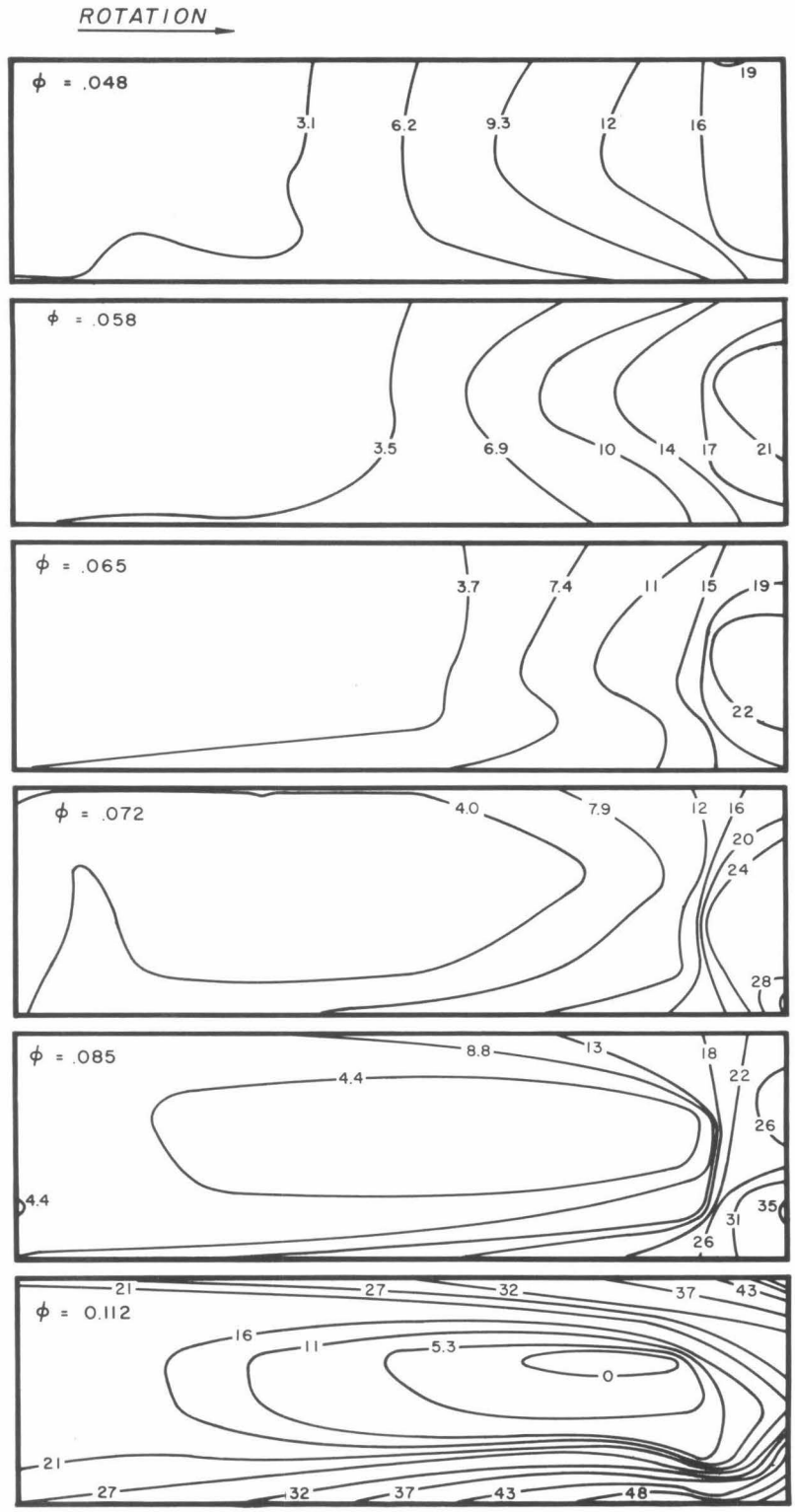

Fig. 19 - Relative total head loss contours for the 12.5° impeller at the mid-radius position ($r/r_2 = 0.89$).

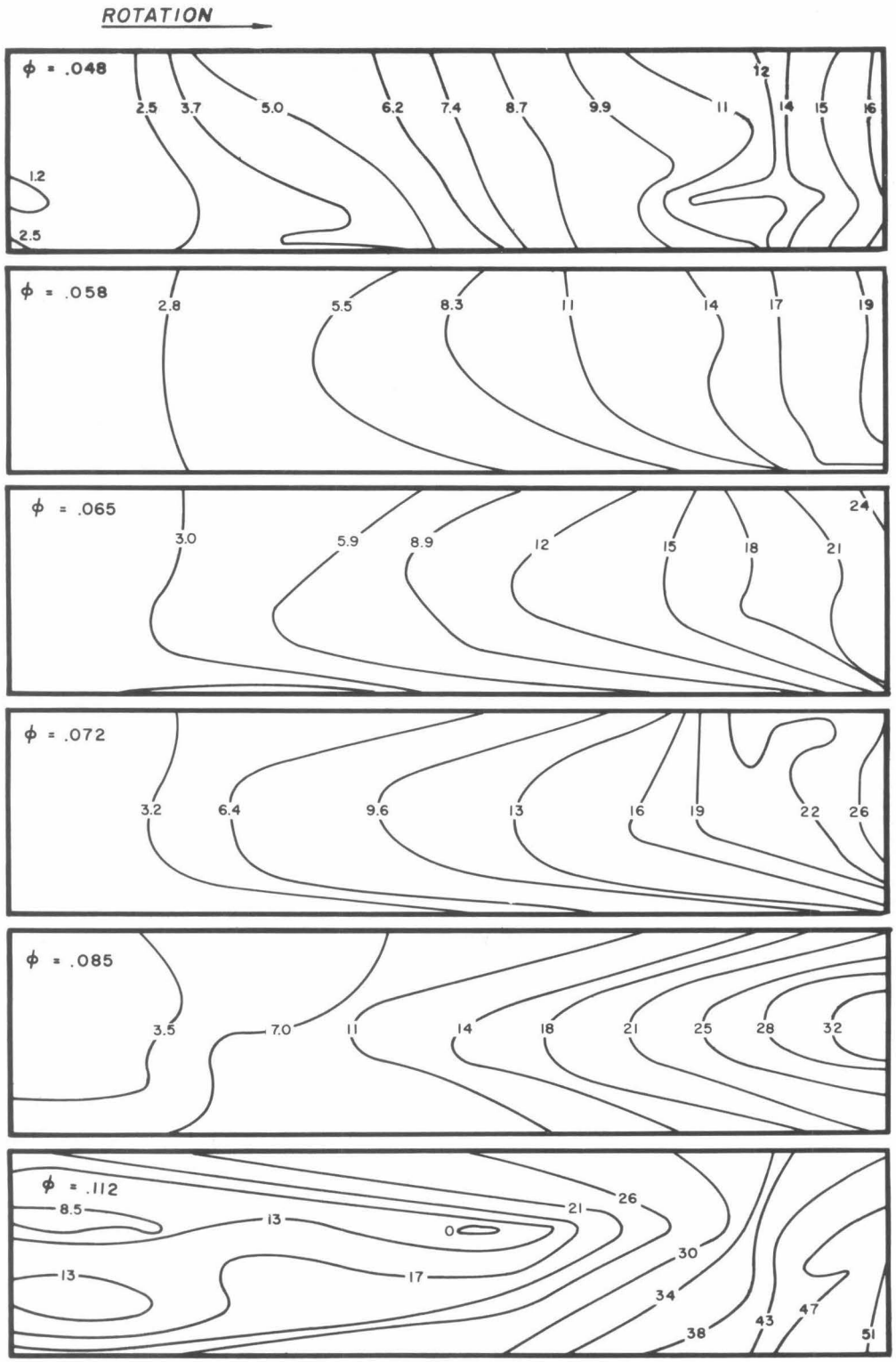

Fig. 20 - Relative total head loss contours for the 12.5° impeller near the inlet ($r/r_2 = 0.73$).

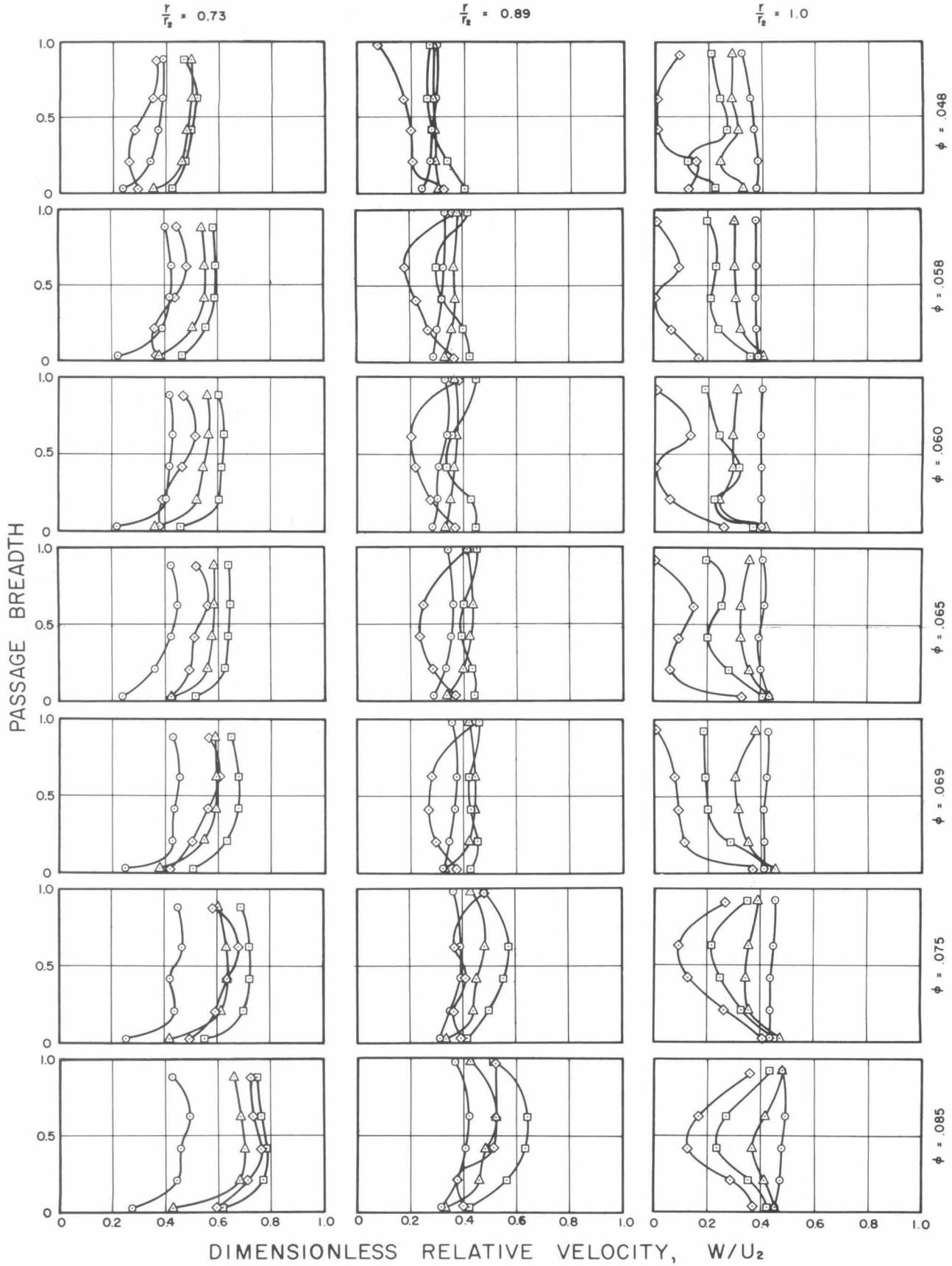

Fig. 21 - Relative velocity profiles for the 12.5° impeller at three radii for several flow rates.

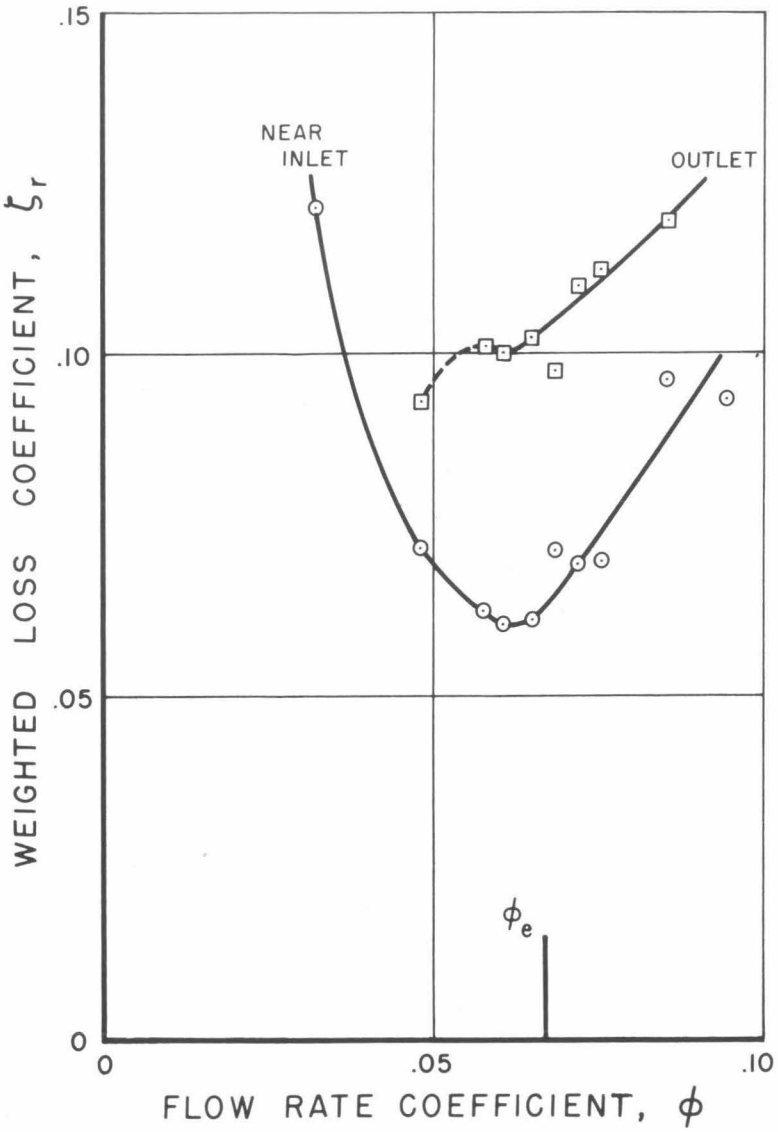

Fig. 22 - Weighted relative total head loss coefficients near the impeller inlet and at the impeller exit for the 12.5° impeller.

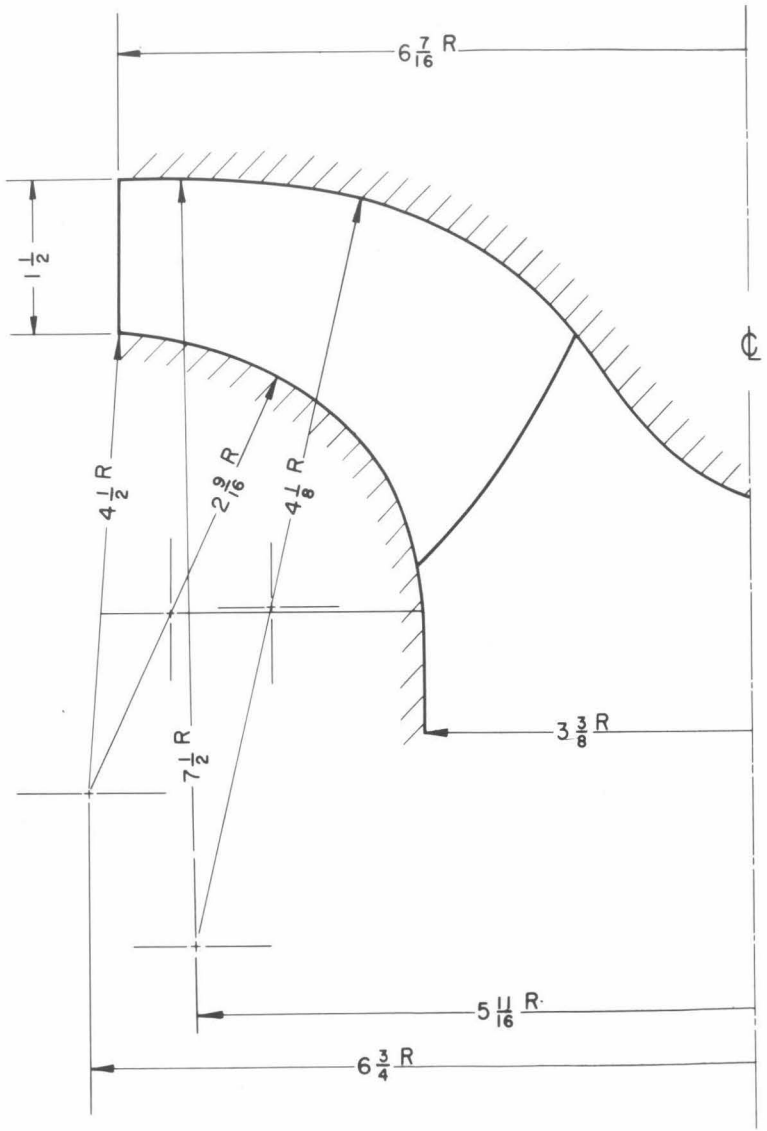

Fig. 23 - Cross-section sketch of the three-dimensional impeller.

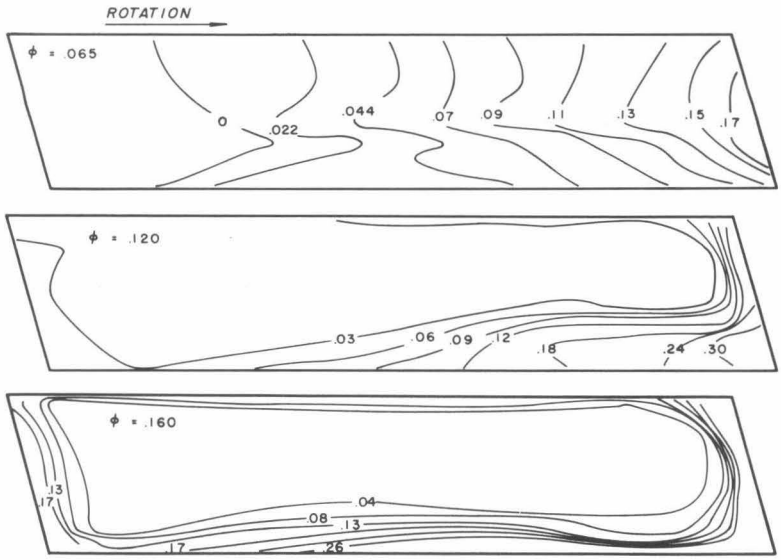

Fig. 24 - Relative total head loss contours for the three-dimensional impeller at the impeller exit.

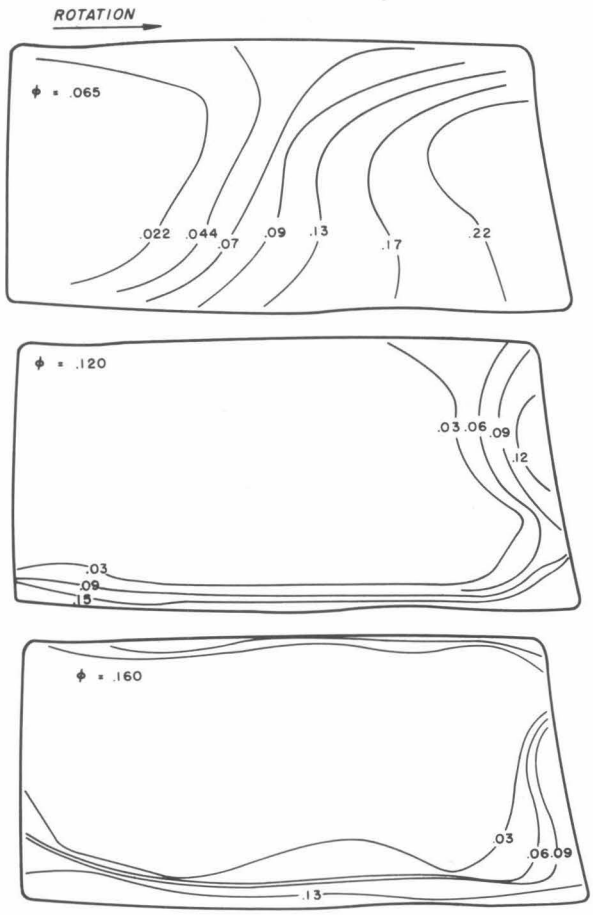

Fig. 25 - Relative total head loss contours for the three-dimensional impeller neat the impeller inlet.

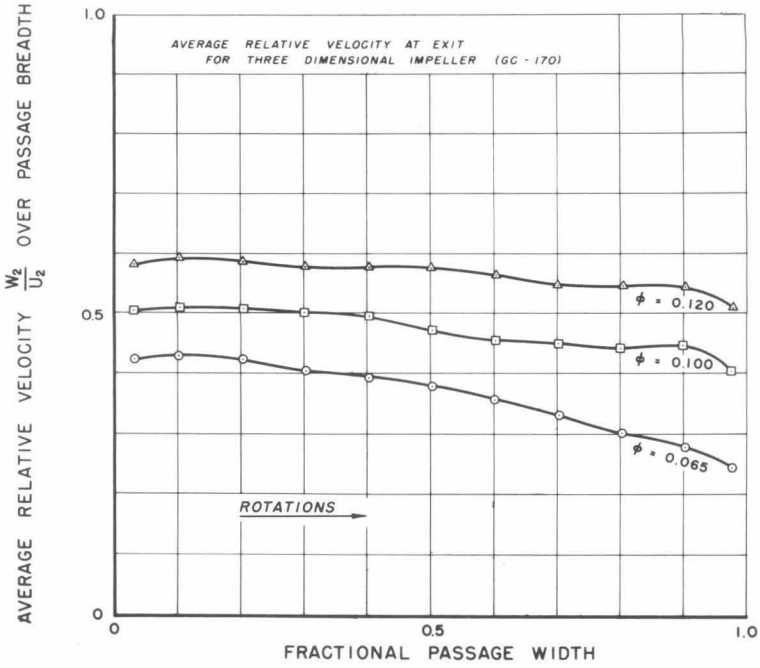

Fig. 26 - Average relative velocity at the impeller exit for the three-dimensional impeller.

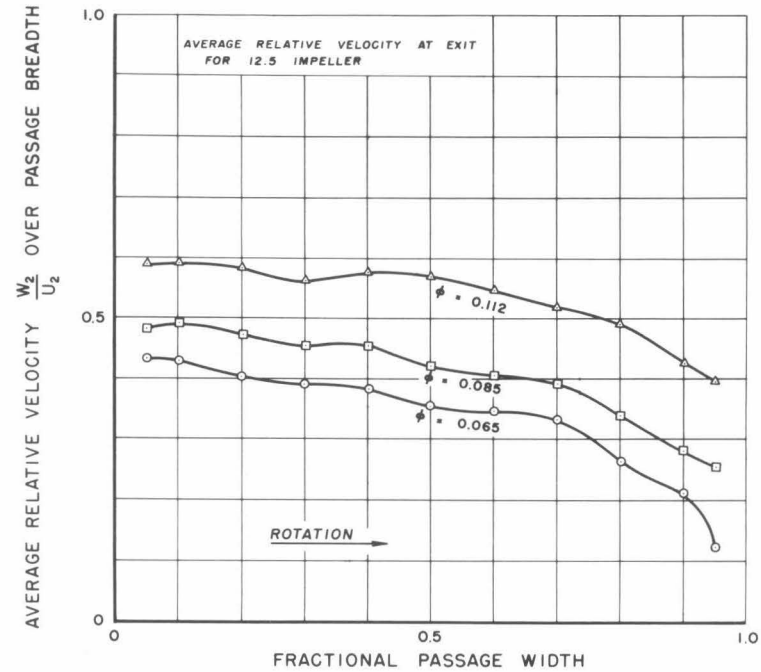

Fig. 27 - Average relative velocity at the exit of the 12.5° impeller.

DISTRIBUTION LIST
CONTRACT N6onr-24402

Chief of Naval Research
Department of the Navy
Washington 25, D. C.
Attn: Code 429 1
" Code 438 2

Commanding Officer
Office of Naval Research
Branch Office
John Crerar Library Building
86 E. Randolph Street
Chicago 1, Illinois 1

Commanding Officer
Office of Naval Research
Branch Office
346 Broadway
New York 13, New York 1

Commanding Officer
Office of Naval Research
Branch Office
1030 East Green Street
Pasadena 1, California 2

Commanding Officer
Office of Naval Research
Branch Office
1000 Geary Street
San Francisco, California 1

Chief, Bureau of Aeronautics
Department of the Navy
Washington 25, D. C.
Attn: Research Division 1

Chief, Bureau of Ordnance
Department of the Navy
Washington 25, D. C.
Attn: Code Re6a 1
Research and
Development Div. 1

Commanding Officer
Naval Ordnance Laboratory
White Oak
Silver Spring, Md. 1

Commander
Naval Ordnance Test Station
3202 E. Foothill Blvd.
Pasadena, California
Attn: Mr. J. Neustein 1

Commanding Officer
Naval Torpedo Station
Keyport, Washington 1

Chief, Bureau of Ships
Department of the Navy
Washington 25, D. C
Attn: Research Div. 1
" : Prop and Shaft Branch 1

Documents Service Center
Armed Services Technical
Information Agency
Knott Building
Dayton 2, Ohio 5

Director
Naval Research Laboratory
Washington 20, D. C.
Attn: Code 2021 1

Commanding Officer and Director,
David Taylor Model Basin
Washington 7, D. C.
Attn: Hydromechanics Lab. 1
" : Hydromechanics Div. 1
" : Ship Div. 1
" : Technical Library 1

Commanding General
Office of Ordnance Research
Department of the Army
Washington 25, D. C. 1

Directorate of Intelligence
Headquarters, U. S. Air Force
Washington 25, D. C.
Attn: Director, Research
and Development 1

Commanding General
Air Research and Development Command
Office of Scientific Research
Post Office Box 1395
Baltimore 3, Maryland 1

Director of Research
National Advisory Com. for Aeronautics
1724 F Street, Northwest
Washington, D. C.
Attn: Director of Research 1

Director
Langley Aeronautical Laboratory
National Advisory Com. for Aeronautics
Langley Field, Virginia 1

Director
Ames Aeronautical Laboratory
National Advisory Com. for Aeronautics
Moffett Field, California 1

Director
Lewis Flight Propulsion Laboratory
National Advisory Com. for Aeronautics
21000 Brookpark Road
Cleveland 11, Ohio 1

Director
National Bureau of Standards
National Hydraulic Laboratory
Washington 25, D. C.
Atth: Dr. G. B. Schubauer 1

Polytechnic Institute of Brooklyn
Department of Aeronautical Engineering and Applied Mechanics
99 Livingston Street
Brooklyn 2, New York
Attn: Professor A. Ferri 1
" : Professor H. J. Reissner 1

Polytechnic Institute of Brooklyn
Department of Mechanical Engineering
99 Livingston Street
Brooklyn 2, New York
Attn: Professor C. H. Wu 1

The Johns Hopkins University
Dept. of Mechanical Engineering
Baltimore 18, Maryland
Attn: Dr. G. F. Wislicenus 1

Massachusetts Institute of Technology
Hydrodynamics Laboratory
Cambridge 39, Mass.
Attn: A. T. Ippen 1

Massachusetts Institute of Technology
Dept. of Naval Architecture
Cambridge 38, Mass. 1

Massachusetts Institute of Technology
Dept. of Mechanical Engineering
Cambridge 39, Mass.
Attn: Prof. E.S. Taylor 1

Ordnance Research Laboratory
Pennsylvania State College
State College, Pennsylvania
Attn: Dr. J. N. Robertson 1

Princeton University
Dept. of Mechanical Engineering
Princeton, New Jersey
Attn: Prof. C. P. Kittridge 1

State University of Iowa
Iowa Institute of Hydraulic Research
Iowa City, Iowa
Attn: Dr. Hunter Rouse, Director 1

Experimental Towing Tank
Stevens Institute of Technology
711 Hudson Street,
Hoboken, New Jersey 1

University of California
Department of Mechanical Eng.
Berkeley, California
Attn: Dr. H. A. Einstein 1

University of Maryland
Institute for Fluid Mechanics and Applied Mathematics
College Park, Maryland
Attn: Prof. J. R. Weske 1

University of Minnesota
St. Anthony Falls Hydraulic Lab.,
Minneapolis 14, Minnesota
Attn: Dr. L. G. Straub 1

University of Notre Dame
College of Engineering
Notre Dame, Indiana
Attn: Dr. K.E. Schoenherr, Dean 1

University of Tennessee
Engineering Experimental Station
Knoxville, Tennessee
Attn: Dr. G. H. Hickox
Associate Director 1

Worcester Polytechnic Institute
Alden Hydraulic Laboratory
Worcester, Massachusetts
Attn: ~~Mr. C. A. Gongwer~~ Prof. L. J. Hooper 1

California Institute of Technology
Jet Propulsion Laboratory
Pasadena 4, California 1

Commanding Officer
Office of Naval Research
Navy 100, Fleet Post Office
New York, New York 1

Editor, Bibliography of Tech. Reports
Office of Technical Services,
U. S. Dept. of Commerce,
Washington 25, D. C 1

Editor, Technical Data Digest,
Armed Services Tech. Information
Agency,
Document Service Center.
U. B. Bldg.,
Dayton 2, Ohio

Editor, Engineering Index,
29 West 39th Street
New York 18, N. Y. 1

Editor, Aeronautical Engineering
Review,
2 E. 64th Street,
New York 21, N. Y. 1

Editor, Applied Mechanics Reviews,
Midwest Research Institute,
4049 Pennsylvania Ave.,
Kansas City 2, Missouri 2

Technical Library,
Lockheed Aircraft Corp.,
2555 North Hollywood Way,
Burbank, California 1

Technical Library,
Pratt and Whitney Aircraft Div.,
United Aircraft Corp.,
East Hartford 8, Conn. 1

Technical Library,
Glenn L. Martin Company
Baltimore 3, Maryland 1

Technical Library,
Grumann Aircraft Engineering Corp.
Bethpage, Long Island, N. Y. 1

Technical Library,
McDonnell Aircraft Corp.,
Box 516,
St. Louis 3, Missouri 1

Technical Library,
Northrop Aircraft Company
1017 E. Broadway,
Hawthorne, California 1

Professor H. Emmons,
Harvard University,
Cambridge 38, Mass.

Hydraulics Laboratory,
Michigan State College,
East Lansing, Michigan
Attn: Prof. H. R. Henry 1

Aerojet General Corp.,
6352 Irwindale Ave.,
Azusa, Calif.
Attn: Mr. C. A. Gongwer 1